Responses to Reviewers 1 and 2

We thank both reviewers for taking time to read the manuscript and provide excellent feedback. The reviewer's comments are in black, responses in blue, and modified text in revised manuscript in *red*.

1 Response to Reviewer 1

1.1 General Comments

This study investigates the influence of mineral dust concentrations on cirrus formation through a series of sensitivity simulations for a single case study, evaluated against multiple observational datasets. In doing so, it establishes a link between cloud microphysics, radiation, and convective dynamics.

While this is an ambitious study, the current version is at times difficult to follow and occasionally lacks some essential information.

We first would like to thank the referee for the thorough and nice review of our manuscript with the detailed comments and questions, which will be addressed point by point below.

G1. Uncertainty and comparability of observational and model datasets: This study draws on multiple observational datasets including satellite retrievals (IWC, ICNC, cloud top temperature), in-situ measurements, and cloud radar data alongside model simulations. Each of these carries its own uncertainties and underlying assumptions, yet these are only in a few cases elaborated upon, leaving it unclear to what degree agreement between the different data sources can reasonably be expected. I suggest that a discussion of these uncertainties and limitations be included either in the methods section or the conclusions.

Response:
We thank the referee for highlighting this issue. We agree that the original manuscript did not sufficiently distinguish between direct in-situ measurements, remote-sensing retrievals, and model-domain statistics, or explain the degree of agreement that can reasonably be expected between them.
We have expanded the statements regarding instrumentation uncertainties in Sections 2.2 and added an interpretation framework within the model-observation comparisons in Sect. 3.1 and 3.2. We now clarify that HALO provides the most direct constraint on the air mass represented by the LES model. DARDAR-Nice and MIRA 35-C provide complementary constraints, but their microphysical properties are retrieval products with assumptions related to particle size distributions, particle-size thresholds, radar-lidar information, and other radar-related relationships. We have further clarified the temporal and spatial sampling differences. The LES state used for the microphysical comparison represents the HALO sampling period at approximately 09:00 UTC, while DARDAR-Nice and MIRA-35C measured at different locations and sampling periods.
We have now extended discussion of discrepancy that ICNC has for model and observations inside the SEDI layer. We do not interpret the closer agreement with DARDAR-Nice as evidence that this retrieval is more accurate, nor do we treat NIXE-CAPS as an uncertainty-free reference. Instead, the difference is discussed as a combined consequence of possible sampling and retrieval differences, limits in model microphysics, sedimentation and vertical wind transport of ice, and temporal evo-

lution of the cloud.
Finally, we added discussion of uncertainty in the ERA5-derived large-scale vertical velocity. This is a model-diagnosed estimate of synoptic-scale ascent, and uncertainty in its amplitude, timing, and vertical structure may affect RHi, ice nucleation, transport, and sedimentation in the SEDI layer. Since only one ERA5 forcing trajectory was used, this contribution could not be quantified independently. The conclusions now state that agreement is strongest in the CONV layer, whereas the SEDI-layer comparison is less conclusive, and that the observations are used as complementary constraints on cloud structure and process consistency rather than as strict point-by-point validation.
We have also added discussion of turbulent mixing and unresolved subgrid-scale variability. Although the LES resolves the larger eddies, turbulent motions below the model grid scale are represented through the subgrid-scale closure model and do not produce explicitly resolved local distributions of RHi. This may be particularly relevant in the weakly convective SEDI layer, where local RHi fluctuations exceed conditions favorable for ice nucleation even when the grid-cell or layer-mean RHi remains close to ice saturation. Consistent with Kärcher et al. (2025), who showed that turbulent RHi fluctuations can promote earlier heterogeneous ice formation and modify subsequent homogeneous freezing through enhanced vapor depletion, we now identify unresolved turbulent mixing as an additional uncertainty in interpreting the SEDI-layer ICNC discrepancy.

Location in revised manuscript: Sect. 2.2, pp. 4–6, lines 110–155; Sect. 2.4, pp. 8–10, lines 195–250; Sect. 3.2, pp. 16–18, lines 335–380; Sect. 3.3.2, pp. 20–22, lines 420–480.

We have provided the tracked changes related to model–observation comparisons in Section 3.1 which now begins with the following:

"3.1 BASE simulation and comparison with observations
In this section, we present results from the BASE and BASE-MIXED simulations and compare the model results against observations. All primary analyses are conducted using the H14 scheme. The U17 and P13 schemes are used to assess the sensitivity of the simulated ice nucleation pathways, with the resulting structural uncertainty in ICNC, IWC, and radiative feedbacks discussed in Sect. 3.3.1. For the model–observation comparisons, NIXE-CAPS measurements provide the primary constraint on the simulated microphysical properties because the BASE simulations were designed to represent the timing and location of the HALO sampling of the dusty cirrus at approximately 09:00 UTC. Although NIXE-CAPS has limited spatial and temporal coverage, it provides direct in-situ measurements and involves fewer retrieval assumptions than the remote-sensing products. DARDAR-Nice and MIRA-35C are therefore used as complementary datasets. They are not precisely co-located with the HALO sampling region in space or time, but they provide independent information on the same dusty cirrus event (approximately similar thermodynamical conditions can be expected) and extend the observational constraint above the approximately 9.5 km limit of the NICE-CAPS sampling."

In Section 3.2, we have added a following text regarding the comparability of NIXE-CAPS measurements to model domain ICNC:

"For ICNC, the vertical profile has a very similar shape to the IWC profile in the CONV layer (Fig. 9b) for both BASE and BASE-MIXED cases. The modeled ICNC varies within a range comparable to that observed by NIXE-CAPS, although the NIXE-CAPS mean ICNC is approximately 1.9× and 1.2× higher than the BASE and BASE-MIXED means, respectively. The comparison of mean ICNC between the model and NIXE-CAPS is, however, subject to sampling uncertainty

because NIXE-CAPS covers only approximately 500 m of the CONV layer, while the agreement is good at the uppermost altitude sampled by the measurements. In the SEDI layer, the mean NIXE-CAPS ICNC is 1.87 $\mathrm{cm^{-3}}$*, compared with 0.24* $\mathrm{cm^{-3}}$ *and 0.25* $\mathrm{cm^{-3}}$ *for BASE and BASE-MIXED, respectively. Thus, the observed mean is approximately 7.8× and 7.5× higher than the modeled means, and the NIXE-CAPS ICNC values exceed the full range simulated within the LES domain. The HALO aircraft had a horizontal footprint of approximately 23–24 km during the ascent between 8 and 8.8 km altitude with a true air speed of roughly 190* $\mathrm{m\,s^{-1}}$*, corresponding to approximately 190 m horizontal sampling resolution for NIXE-CAPS. This is comparable to the LES model domain horizontal extent of 24 km and its 150 m horizontal resolution, providing good scale-wise comparability. The lack of similarly high ICNC values in the model and NIXE-CAPS measurements within the SEDI layer suggests that processes in the model setup or microphysical treatment may contribute to the difference. This is discussed further in Sect. 3.3."*

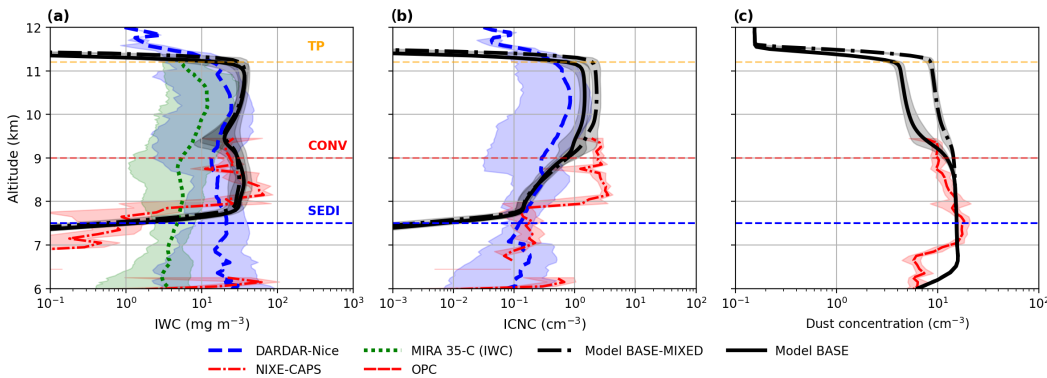

Figure 1: (in revised manuscript Fig. 9) BASE and BASE-MIXED simulation results (black solid and dash-dotted lines) compared with DARDAR retrievals (blue dashed), cloud radar MIRA-35C observations at Schneefernerhaus (green dotted), and in situ NIXE-CAPS measurements (red densely dash-dotted) of (a) ice water content (IWC), (b) ice crystal number concentration (ICNC), and (c) dust number concentration from OPC. UCLALES-SALSA results represent the final model time step at 09:00 UTC with 150 m horizontal and 50 m vertical resolution, with model lines showing spatial means within each altitude bin. DARDAR retrievals correspond to the CloudSat overpass at 12:30 UTC over the latitude range 47–49°N. MIRA-35C IWC observations at Schneefernerhaus (47.417°N, 10.977°E) are time-averaged over 06:00–08:00 UTC at 30 s resolution, the period closest to the NIXE-CAPS measurements. The NIXE-CAPS ICNC profile represents the vertical ascent of HALO between 09:15 and 09:25 UTC with 1 Hz sampling that corresponds to approximately 190 m horizontal resolution, with measurements binned into 100 m altitude intervals. All lines represent mean values within their respective altitude bins. Shading indicates the 5th–95th percentile range for each data measured, retrieved or modeled.

In Section 3.2, we have added a following text regarding the uncertainty related to comparion of DARDAR-Nice to model results with following:

"Although the DARDAR-Nice and model ICNC profiles agree reasonably well, the larger NIXE-CAPS ICNC values in the SEDI layer cannot be uniquely attributed to model processes. The model is forced along a single ERA5-derived trajectory between 03:00–09:00 UTC, while DARDAR-Nice provides observations from the 12:30 UTC CloudSat overpass. The final model state was selected to have a thermodynamic state comparable to that observed during the CloudSat overpass, providing a useful basis for comparison, but the difference in sampling time means that the observations and

model do not necessarily represent the same stage of cloud evolution. These differences should therefore be considered when interpreting the agreement and discrepancies between the model and observational datasets. The difference in ICNC measured from different observation techniques gives some indication of the level of observational uncertainty. Given the model ICNC is found within this range, it gives some confidence in the model."

G2. Role of sedimentation: Heterogeneously formed ice crystals in particular are associated with high sedimentation fluxes. This study does not sufficiently discuss whether ice crystals observed at a given altitude were actually formed there, nor the potential role of sedimentation in the vertical redistribution of ice. While the averaging approach and statistical presentation adopted here may largely mitigate the influence of sedimentation on the interpretation of the results, this should be discussed more explicitly.

Response:
We thank the referee for pointing out that the role of sedimentation required a more explicit discussion, as heterogeneously formed cirrus clouds are known to be impacted significantly by sedimentation. We agree that ice observed at a given altitude cannot necessarily be assumed to have formed locally, particularly in the lower SEDI layer.
We have expanded the discussion in new Section 3.3. The SEDI layer is now explicitly described as a region where ice is influenced by large-scale ascent and by ice crystals sedimenting from the convectively active layer above. To quantify the role of sedimentation, we added an ICNC tendency analysis (Fig. 2) based on the model outputs separating the contributions from deposition ice nucleation, sedimentation, vertical transport by turbulent winds, and sublimation. The analysis shows that DIN is the dominant source of ICNC in the CONV layer, whereas sedimentation dominates the ICNC tendency in the SEDI layer.
We additionally discuss uncertainty in the simulated sedimentation flux. The model uses a simplified representation of ice habits, with spherical particles at smaller sizes and bullet rosettes at larger sizes, whereas observations such as Lawson et al. (2019) show a broader range of particle habits. Consequently, the assumed particle shapes and terminal velocities may underestimate or overestimate sedimentation and the resulting ICNC in the SEDI layer. The NIXE-CAPS size distributions, including the abundance of small crystals, are consistent with recent ice nucleation, but do not uniquely identify whether those crystals formed locally or were transported from above.

Location in revised manuscript: Sect. 3.3.2, pp. 20–22, lines 420–480.

Below you can find the revised Section 3.2.2 which now addresses ICNC uncertainty in SEDI layer from sedimentation to other microphysical to dynamical aspects:

*" **3.3.2 Possible sources of the ICNC uncertainty***
The results above show the choice of DIN parameterization strongly affects the simulated ICNC. However, the remaining discrepancy between simulated and observed ICNC in the SEDI layer cannot be attributed to DIN alone. As discussed in Sect. 3.2, differences in sampling location and time, the limited vertical coverage of NIXE-CAPS, and differences in measurements and retrieval characteristics introduce observational and representativeness uncertainties into this comparison. These uncertainties prevent the discrepancy from being uniquely attributed to model deficiencies, but they do not exclude contributions from model-related processes. In this subsection, we examine additional process-level uncertainties in the representation of ice growth, sedimentation, sublimation, and homogeneous freezing. We then discuss uncertainties associated with the model inputs and experimental design, including the ERA5-derived large-scale vertical velocity and the representation

of subgrid-scale turbulence.
To grasp the full picture of how the ICNC is controlled in the modeled dusty cirrus, we examine the ICNC tendencies to assess the contribution of these processes. Figure 12 shows the contributions of DIN, sedimentation, vertical transport, and sublimation to the ICNC tendency at different levels for the H14 simulation. Overall, DIN is the dominant source of ICNC within the CONV layer. Ice nucleation rates for immersion and homogeneous freezing were not included due to the rates for those were at zero. Sublimation, in contrast, provides the strongest sink of ICNC in the lower half of CONV, particularly at levels associated with the descending branches of convection, where RHi is also likely to be the lowest. Vertical transport exhibits a net negative ICNC tendency in the upper half of CONV and a positive tendency in the lower half. Interestingly, the vertical transport profile closely reflects the structure of the descending branches. When the transport is separated into ascending and descending branches, the local tendencies associated with vertical transport can be substantially larger than those of the other processes. Near the cloud top, upward vertical transport increases ICNC by lifting ice crystals towards the tropopause, while sedimentation produces an opposing tendency as the ice crystals subsequently fall back towards lower levels. Thus, the vertical transport and sedimentation tendencies exhibit opposing profiles near the cloud top. Despite the large local contributions of individual processes, their net ICNC tendencies within CONV are relatively homogeneous throughout the layer.

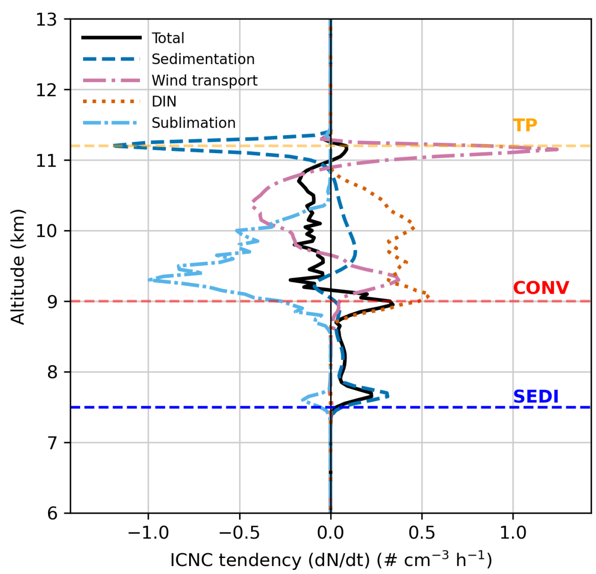

Figure 2: (In revised manuscript Fig. 12) Horizontal mean tendency of ICNC as a vertical profile at the last time step of the BASE simulation.

On the other hand, sedimentation dominates the ICNC tendency in the SEDI layer, as expected. DIN does not contribute substantially to new ice formation because H14, U17 or P13 produces little additional ice under conditions close to ice saturation. One possible cause for the lower ICNC in the H14 simulations compared with NIXE-CAPS observations is an underestimation of sedimentation velocities. UCLALES-SALSA uses a relatively coarse representation of ice crystal habits, with only bullet rosettes considered for particles larger than 40 μm. *Although large in-situ cirrus crystals are often dominated by rosette-type habits, Lawson et al. (2019) also reported substantial populations of irregular and spheroidal crystals above 40* μm. *The sedimentation parameterization for bullet rosettes with a maximum diameter of 100* μm *gives terminal velocities approximately four* *times lower than those of spherical particles of the same size (Sölch and Kärcher, 2010, Fig. A1). A larger contribution from faster-falling spherical and irregular crystals could therefore increase sedimentation flux and modify ICNC in the SEDI layer. Interestingly, NIXE-CAPS measurements show a similar ice PSD shape throughout the SEDI layer between 8 and 9.5 km (Supplementary Fig. S8). We estimate that ice crystals of size 20* µm *have terminal velocity of only approximately 2* $\mathrm{cm\,s^{-1}}$*, corresponding to a fall distance of about 72 m* h^{-1}*. Together with the conditions near ice saturation in SEDI (Fig. 3a), this low fall speed makes persistence of the small ice crystals physically plausible, as the mean depositional growth or sublimation rate would be small. At the same time, a broad tail in ice PSD in Fig. 10a is indicative of sedimentation affecting the PSD.*

Another mechanism beside DIN at cirrus conditions for ice nucleation is homogeneous freezing. At the temperatures considered, however, homogeneous nucleation would require RHi values of approximately 140–150%, with the threshold increasing with decreasing temperature. In the BASE simulations, efficient DIN and sedimentation reduces RHi before this threshold is reached, effectively suppressing homogeneous freezing. As a result, homogeneous freezing did not contribute to the ICNC in the BASE simulation. For example, in the BASE simulation (Fig. 13a), large-scale ascent increases RHi up to about 110% below 9 km (SEDI), but sedimentation from above and in-situ ice formation limit further increase in RHi, preventing the onset of homogeneous freezing. A similar sedimentation-related suppression and homogenization of RHi was reported by Kärcher et al. (2025): RHi exhibited substantially greater variability when sedimentation was omitted than when it was included. Within the CONV layer, DIN and sedimentation maintain RHi near saturation over ice due to large ice nucleation active dust particles.

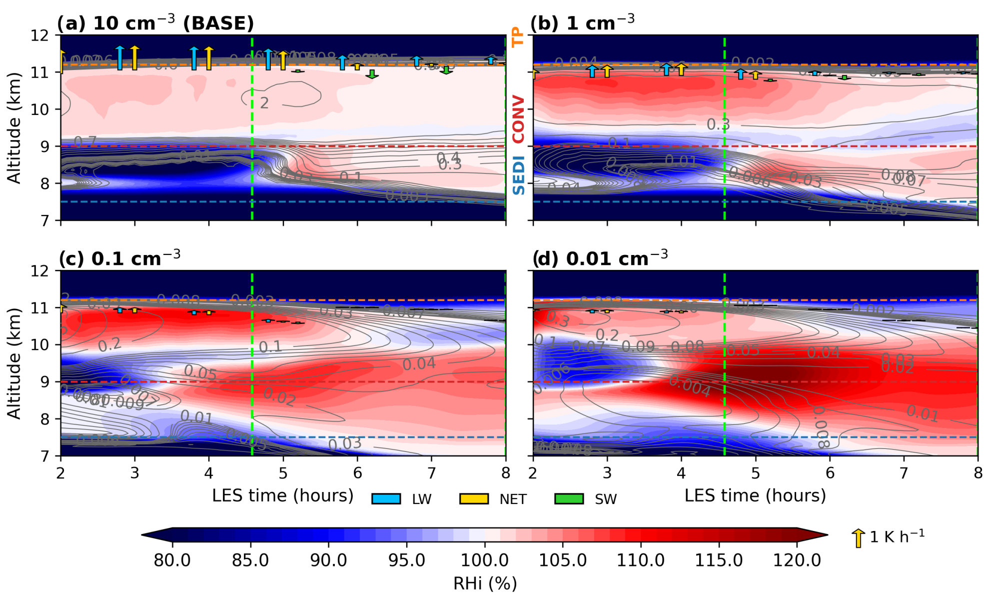

Figure 3: (In revised manuscript Fig. 13) Horizontal means of RHi (shading) and ICNC (contours, cm^{-3}) within the cirrus for different initial N_D in descending order (a)-(d). The green dashed vertical line indicates the onset of SW radiation. Upward yellow arrows indicate the maximum net radiative cooling at the cloud top, LW cooling in blue arrows and SW heating in downward green arrows.

In addition to these process-level uncertainties, the comparison is affected by uncertainty in the *imposed ERA5-derived w_{LS}. This uncertainty may be particularly important for ICNC in the SEDI layer, where resolved convective motions are weaker than in the CONV layer and large-scale ascent strongly influences the temperature and RHi evolution. Figure 13a shows that ICNC varies substantially in the SEDI layer during the BASE simulation, whereas it remains comparatively stable in the CONV layer, suggesting that the SEDI layer is more sensitive to the evolving large-scale forcing. The actual large-scale ascent may have differed from the ERA5 trajectory, producing periods of stronger ascent, higher RHi, and enhanced ice nucleation in the SEDI layer. A further limitation is that turbulent motions below the LES grid scale are represented through the subgrid-scale closure rather than explicitly solved. Such fluctuations could produce local pockets of RHi that are smoothed within a grid cell, potentially creating conditions favorable for DIN even when the resolved RHi remains close to ice saturation. Kärcher et al. (2025) reported that, for efficient INPs such as mineral dust, turbulent supersaturation fluctuations can promote earlier heterogeneous ice formation, thereby enhancing vapor depletion and reducing subsequent homogeneous freezing. As the LES used in this study does not explicitly resolve subgrid-scale turbulence, its effect on the microphysics cannot be quantified in this study."*

G3. Readability of the manuscript: The manuscript addresses the complex interplay between cloud microphysics, radiative cooling and heating, and convective dynamics, drawing on data from sensitivity simulations and several distinct observational datasets. For readers who are not experts across all of these areas, the manuscript can be difficult to follow. I therefore recommend investing some effort in restructuring parts of the manuscript, elaborating on key concepts where necessary, and clarifying the connections between them. For example, by more clearly delineating subsections and revisiting the ordering of the large amount of figures. My specific comments below may offer some guidance in this regard.

A list of abbreviations in the appendix would also be helpful.

Response:
We have substantially reorganized the manuscript to improve readability and clarify the links between cloud microphysics, radiation, and dynamics in current Section 3.4 (was 3.2). Please find the revised text below in response to RC1-S24. Section 3 is now divided by removing excessive subsub Sections and added relevant subsections for explaining sensitivities to radiation and large-scale forcing. We also revised the figure order and captions, clarified model setup and observational datasets to help understanding key concepts in Sections 2.2–2.4. These changes are specified in the responses more explicitly on the specific comments below. We have added an appendix listing abbreviations and variables that is found at the bottom of this response letter.

Location in revised manuscript: Appendix A, pp. 34–36, Tables A1–A2.

The list of abbreviations and variables are given at the bottom of this response letter and located in the Appendix of the revised manuscript:

1.2 Specific Comments

S1. Line 58-59: Consider providing a reference or including the particle growth equation in the appendix.

In Appendix B, we added: We now label the particle growth equation as Eq. B1 and ice growth equation as Eq. B2 and define all variables appearing in them. The equivalent potential temperature equation is consequently Eq. B3, and its variables are also defined.

Location in revised manuscript: Appendix B, p. 37, lines 705–725.

" For growth and evaporation of particles in SALSA, mass transfer is calculated for single particles in the following form in Jacobson (2005) (Eq. 16.13).

$$\frac{dm}{dt} = \frac{4\pi r D_q' \left(p_q - p_{q,s}'\right)}{\dfrac{D_q' \, L_{e,q} \, p_{q,s}'}{\kappa_a \, T} \left(\dfrac{L_{e,q} m_q}{R^* T} - 1\right) + \dfrac{R^* T}{m_q}} \tag{1}$$

where m is the mass of particle, r is its radius, D_q' is the effective diffusivity of water vapour, p_q is the ambient water-vapour partial pressure, and $p_{q,s}'$ is the corresponding effective saturation vapour pressure at the particle surface. $L_{e,q}$ is the latent heat associated with water-vapour transfer, κ_a is the thermal conductivity of air, T is temperature, m_q is the molecular mass of water, and R^* is the universal gas constant. The primes denote effective quantities used in the particle-growth formulation. This equation is further modified to ice particles in the following form (Eq. 16.76):

$$\frac{dm_i}{dt} = \frac{4\pi \chi_i D_{v,i}' \left(p_q - p_{v,s,i}'\right)}{\dfrac{D_{v,i}' \, L_s \, p_{v,I,i}'}{\kappa_{a,i} \, T} \left(\dfrac{L_s}{R_{\mathrm{V}} T} - 1\right) + R_{\mathrm{V}} T} \tag{2}$$

where m_i is the mass of ice particle, χ_i is the crystal electrical capacitance, $D_{q,i}'$ is the effective diffusivity of water vapour over ice, and $p_{v,I,i}'$ is the corresponding effective saturation vapor pressure at the ice surface. L_s is the latent heat of sublimation, and $R_{\mathrm{V}} T$ is the gas constant of water vapor. The primes denote effective quantities used in the particle-growth formulation."

S2. Line 63-64: The setup of aerosols, cloud droplets and ice classes in the bin scheme is still unclear to me. Consider expanding the description.

Response:
Corresponding paragraph in Sect. 2.1 was re-written to clarify the set up of particle bin schemes. The modified paragraph has now following text:

Location in revised manuscript: Sect. 2.1, p. 3, lines 65–80.

"Aerosols and cloud droplets are represented using a dry-bin approach with two parallel bin structures, in which particle number and chemical composition are tracked according to dry particle size. The parallel binning allows two internally mixed aerosol populations to be tracked simultaneously, enabling the separate treatment of soluble and insoluble aerosol species. When coagulation is enabled, aerosols occupying different parallel bins can undergo internal mixing, allowing the composition of the aerosol population to evolve. Ice and precipitation in SALSA are described with a single set of bins with particles assigned to each bin by their wet diameter."

S3. Line 68-70: Is the Koop et al. (2000) rate used for droplet of all sizes and thermodynamic regimes as the specific mention of cloud and raindrops would suggest? The Koop et al. (2000) rate should only be used for nanometer-sized aqueous solution droplets at temperatures below the homogeneous freezing regime of pure water ($T < 235$ K). For micrometer-sized 'pure' water droplets the nucleation rate from Koop and Murray (2016) is appropriate.

Response:
Soluble aerosols considered in this study are nanometer-sized aqueous solution particles, not micrometer-sized. This can be seen original Figure 11. This justifies the use of the Koop et al. (2000) rate. The

mode of the log-normally distributed aqueous solution droplets was 50 nm with standard deviation of sigma=1.4. Also, no cloud or rain droplets were present in the dusty cirrus under temperatures below 235 K. We have changed the sentence introducing homogeneous freezing parameterization in the following way:

Location in revised manuscript: Sect. 2.1, p. 3, lines 80–81; Sect. 2.4, p. 12, lines 270–275.

"In this study, we use the approach of Koop et al. (2000) for homogeneous freezing of aqueous solution droplets formed by water uptake onto soluble aerosol particles. This approach works as the particles participating in homogeneous freezing in SALSA are nanometer sized aqueous solution droplets."

S4. Line 79-80: Is turbulent mixing of aerosols considered in the model?

Response:
Aerosols can mix turbulently via subgrid scale mixing (diffusion). We utilized Smagorinsky subgrid scale model (Smagorinsky, 1963) in this study for the simulations. We added a following clarifying sentence:

Location in revised manuscript: Sect. 2.1, p. 3, lines 79–80.

"Turbulent mixing of particles is modeled using sub-grid scale Smagorinsky (Smagorinsky, 1963) model."

S5. Line 86-89: In typical formulations of the vapor deposition growth equation, the capacitance parameter has the dimensions of a length. It is unclear why this is treated as a constant rather than as a function of ice crystal size or mass. As noted above, referencing the growth equation explicitly would help clarify this choice.

Response:
Capacitance was reported here in the wrong way and should have been written as C/D_{max} for clarity. Inside SALSA, D_{max} is used to multiply capacitance multiplier. For spherical ice, multiplier is 0.5, for larger ice and in this case study for bullet rosettes it was 0.25. In Sect. 2.1, the revised text changes the capacitance to:

Location in revised manuscript: Sect. 2.1, p. 4, lines 95–105.

"The capacitance parameter is set to $C = 0.5D_{max}$ for ice crystals smaller than 20 µm and to $C = 0.25D_{max}$ for ice crystals larger than 50 µm based on (Westbrook et al., 2008). Value for large ice crystals corresponds to bullet rosettes with 4-branches with aspect ratio in the order of 3-5 and with 6-branches in the order of 5–8 (Westbrook et al., 2008)

S6. Line 90: Provide further details of the assumptions underlying the radiation scheme. For example, does it use bulk quantities such as mean particle size, or is it size-resolved? Is the assumed ice particle shape consistent with those used for growth by vapor deposition (spherical and rosettes)?

Response:
Radiation scheme uses bulk quantities, such as ICNC and IWC and effective radius of ice which is calculated using ICNC and IWC. For radiation, the effective radius of ice does not take account the habit of ice unfortunately so some uncertainty is produced here. Aerosol direct radiation,

however, is slightly different where the radiation is calculated separately for each size bin and aerosol composition. Here is the modified text in the manuscript:

Location in revised manuscript: Sect. 2.1, p. 4, lines 105–110.

"For dust-ice cloud-radiation interactions, Fu and Liou (1993) based radiation solver is used where the solver calculates ice cloud interaction with radiation using model grid IWC and effective radius of ice (calculated from ICNC and IWC). For ice, the habit is not accounted in radiation interaction. Aerosol-radiation interaction on the other hand is calculated for each size bin and aerosol species."

S7. Section 2.2.1: Are shattering artifacts, arising from ice crystals breaking up upon entering the cloud probe, a source of uncertainty for ICNC in this dataset?

Response:
NIXE-CAPS probe is designed to prevent shattering within operational conditions (Krämer et al., 2020) so shattering was not considered to affect ICNC significantly in this case. This was addressed in Sect. 2.2.1 in the following way:

Location in revised manuscript: Sect. 2.2.1, p. 5, lines 120–128.

"The NIXE-CAPS had an anti-shattering inlet to avoid counting of ice crystals produced by shattering (Krämer et al., 2020)."

S8. Section 2.5: The setup and general design of the UCLALES simulation would benefit from further clarification. In particular: is the model best understood as an air parcel simulation, but discretized over a three-dimensional domain rather than the zero-dimensional framework of a conventional box model? Is the initial thermodynamic state horizontally homogeneous? Given that the domain already extends from the surface to 14 km, is the domain itself lifted by the vertical wind profile, is adiabatic forcing applied as in a typical box model simulation? Please also specify the boundary conditions. Addressing these points should make the section more accessible to readers unfamiliar with this modeling approach.

Response:
SALSA is applied locally within each Eulerian grid cell as a 0D microphysics model, but the LES simulation as a whole is a true 3D cloud resolving model, not an ensemble of independent air-parcel/box-model simulations.
The initial thermodynamic state is prescribed from a one-dimensional atmospheric sounding and applied uniformly across the horizontal domain, such that temperature, humidity, and pressure initially vary only with height. To introduce horizontal variability and initiate the development of three-dimensional flow structures, a random perturbations are subsequently applied to the temperature field.
Large-scale vertical motion is represented through prescribed tendencies to temperature, humidity, and scalar fields. The vertical motion forcing is applied to model levels, resulting in the adiabatic forcing.
The horizontal boundaries are periodic for both dynamical and scalar fields. At the lower boundary, a no-slip condition is applied together with the surface parameterization. At the upper boundary, a sponge layer is used to damp vertically propagating disturbances; in the present simulations, the sponge layer comprises five Newton-relaxation points. Aerosol and atmospheric particles reaching the surface through wet deposition are removed from the domain.
In Sect. 2.1, the sentence beginning was modified:

Location in revised manuscript: Sect. 2.1, p. 3, lines 55–62; Sect. 2.4, pp. 8–10, lines 195–250.

"UCLALES is an atmospheric LES model" was expanded with: "that works as Eulerian large-eddy simulation where SALSA microphysics is applied locally within each model grid cell. The model domain thermodynamic state is initialized using a one-dimensional atmospheric sounding profile. A random perturbation is then subsequently applied to the temperature field, which initializes turbulent motions. Model boundaries are periodic in horizontal directions, which applies to both wind and scalar fields. Model top contains a sponge layer with adjustable number of Newton relaxation points."

S9. Line 189: Which threshold is being referenced? Koop et al. (2000) does not provide a (singular) ice supersaturation threshold for nucleation.

Response:
The line corresponds to equation given in Ren and Mackenzie (2005), based on a fit to Koop et al. (2000) data at homogeneous nucleation rate coefficient at 10^{10} cm^{-3}s ^{1}. In the revised caption of Fig. 3, we specify:

Location in revised manuscript: Fig. 3 caption, p. 9, lines 210–215.

"The dotted line in panel b) indicates the homogeneous freezing threshold corresponding to Koop et al. (2000) (equation from Ren and Mackenzie (2005))."

S10. Line 231-232: Briefly summarize the mechanisms responsible for the mixing described in the referenced theory. If the mixing arises from cirrus cloud processes themselves, it is worth considering whether the BASE-MIXED profile is an appropriate initial condition for simulations prior to cirrus formation.

Response:
We thank the referee for raising this point. We agree that the interpretation of the BASE-MIXED profile requires clarification. The simulations are not intended to reproduce the complete formation history of the dusty cirrus from a pre-cirrus atmospheric state. Rather, they are initialized to represent the already established dusty cirrus observed during the measurement period, and are used to investigate its subsequent microphysical and dynamical evolution and persistence.

Reconstructing the complete formation of the observed dusty cirrus would require knowledge of the preceding aerosol transport, vertical redistribution, and cloud formation history. Such information is not available from the observations used to constrain our simulations. In particular, the vertical distribution of mineral dust above approximately 9.5 km is not directly constrained by the available in-situ measurements. We therefore prescribe the observed dust distribution as an initial condition and investigate the sensitivity to its unconstrained vertical extent using the BASE and BASE-MIXED configurations.

In this context, BASE-MIXED does not imply that cirrus-induced mixing must have occurred before cloud formation. Instead, it represents an alternative initial state consistent with an already developed and potentially vertically mixed dusty cirrus system. The purpose of this case is to test the sensitivity of the subsequent cloud evolution to the uncertain initial dust distribution above the observationally constrained region. We have clarified this distinction in the manuscript in the following:

Location in revised manuscript: Sect. 2.4, p. 12, lines 260–275.

"Because the simulations are initialized to represent the already established dusty cirrus observed during the measurement period, rather than its complete formation history, the vertical distribution of mineral dust within the cirrus layer is not fully constrained by observations. In particular, direct dust measurements are available only up to approximately 9.5 km, leaving the dust concentration above this altitude uncertain. We therefore consider two vertical configurations. In the BASE configuration, constant N_D is applied between 6 and 9.5 km, whereas in the BASE-MIXED configuration, the same concentration is extended up to 11 km (Fig. 3b). The BASE-MIXED configuration represents a sensitivity case in which dust is distributed throughout the cirrus layer and is additionally motivated by the mixing hypothesis proposed by Seifert et al. (2023), which suggests that mineral dust can become vertically homogenized throughout the cirrus layer during its evolution. These two configurations allow us to assess the sensitivity of the simulated cirrus evolution to the uncertain dust distribution above 9.5 km."

S11. Figure 6: Use different markers for CONV and SEDI layer thresholds.

Response:
Guiding text was added above the threshold lines as shown in Fig. 4 We have also revised the color scheme of panels (a-d) to more color-blind friendly pallette.

Location in revised manuscript: Fig. 6 caption, p. 13, lines 295–300.

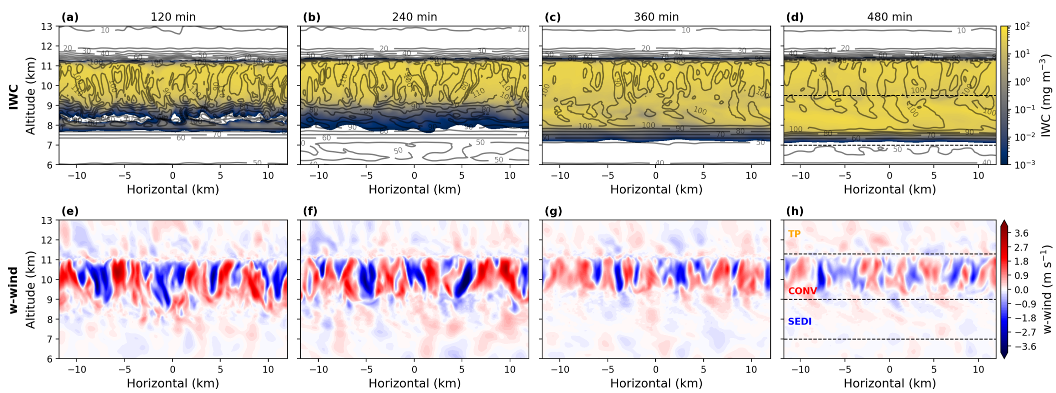

Figure 4: (In revised manuscript Fig. 6) UCLALES-SALSA simulated IWC (upper panels, a-d) and vertical velocity component of wind (lower panels, e-h) at 2 hours time intervals (columns) during the BASE run. At last time step (480 min), TP, CONV and SEDI layer altitudes are marked with dashed lines. Black contours in (a-d) represent RHi at 10% interval.

S12. Line 256-257: Specify the exact region (in time, and horizontal and vertical extent) to which this statement refers. It is not apparent from the figure where the enhanced and reduced IWC values are located — between 9 and 11 km, IWC appears to be close to 10 mg m^{-3} throughout, with no clear correspondence to the regions of elevated updraft or downdraft.

Thank you for pointing out. It is true that IWC values have no clear correspondence to the updrafts and downdrafts. For this reason, we have removed the claim that IWC is related to vertical velocity direction. I have added a Figure for reference below which shows how IWC, ICNC and RHi are roughly related to vertical wind velocity inside the model domain. One can notice that there is a high correlation between RHi and vertical velocity but for IWC and ICNC, the correlation is clearly weaker. It is true that highest IWC and ICNC values are generally found in upward vertical wind branches of dusty cirrus cells which was the intent of the text associated with the new Fig.

6, however, the relationship is too weak to result in any significant shading difference. In fact the relationship between IWC and vertical winds is not also clearly evident in new Fig. 4 (Fig. 4).

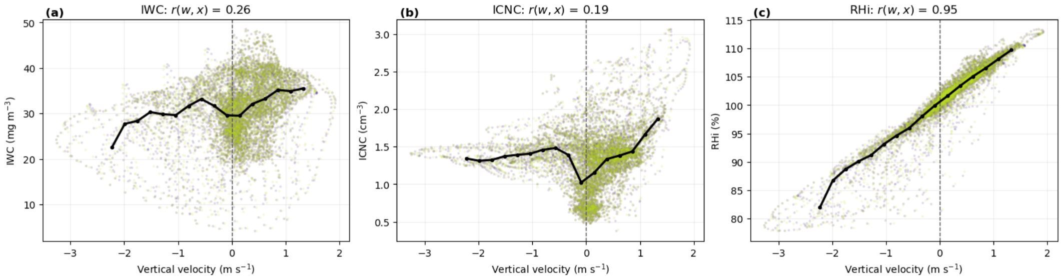

Figure 5: (a) IWC, (b) ICNC, (c) RHi respective to vertical wind in the model domain at the last time step in BASE simulation.

S13. Figure 7: Clarify how the plotted heating rates are calculated. Are they horizontal averages? Additionally, explain the distinction between the shaded regions of high and low transparency.

Response:
Yes, they are horizontal averages of the rates (calculated from fluxes and tendencies), which is now clarified in the caption. The revised Fig. 7 caption reads:

Location in revised manuscript: Fig. 7 caption, p. 14, lines 310–315.

"Horizontal mean heating rates for each term presented in Eq. B3 excluding the large-scale forcing in the BASE run (a-f). Magnitudes of heating rates are shown with shading from blue (negative rate) to red (positive rate)."

S14. Line 271: The reference of Fig. 7 seems incorrect as this figure does not show vertical velocities. Is the reference supposed to be Fig. 6?

Response:
The slowdown in visible in Fig. 7e where turbulent mixing decreases after 5 hours. For clarity, the sentence was modified in following way:

Location in revised manuscript: Sect. 3.1, p. 14, lines 305–315.

"While the SW radiation did not disrupt the convection to the point of collapse, clear slowdown is seen in Fig. 7e as a reduced turbulent mixing after 5 hours. Also, the thickening of the cirrus layer and spreading out of the LW warming after 5 hours, which was caused by the w_{LS} forcing, meant that the net heating rate within the CONV layer decreased. The impact of radiation on dusty cirrus evolution is more closely discussed in Sect. 3.5."

S15. Line 274: Is the reference supposed to be Fig. 6? If not, indicate the CONV layer in Fig. 7 as well.

Response:
It is supposed to be Fig. 7 and we added layer markers as suggested.

Location in revised manuscript: Fig. 7 caption, p. 14, lines 310–315.

S16. Figure 8: Are these horizontally averaged vertical velocities?

Response:
No horizontal averaging, statistical frequency at levels mentioned in the figure. MIRA-35C doppler velocities were additionally filtered to remove the background ice sedimentation velocities and calculate air velocity estimation using two hour windowed averages of Doppler velocities. The revised Fig. 8 caption reads:

Location in revised manuscript: Fig. 8 caption, p. 15, lines 320–325.

"Model vertical wind frequency distribution compared with in-situ measurements at 9.5 km and MIRA-35C Doppler velocities at 9.5 and 10.5 km. 2 hour moving average was used to reduce the effects of sedimentation, Doppler velocities, reflecting closer to air velocity. The derivation of air velocity from Doppler velocities follows method for running-mean technique presented in Protat and Williams (2011)."

S17. Figure 9: Clarify what the panel labels (e-h) indicate in the sub-caption since the first time this figure is referenced in Section 3.1 this is not clear. Where in the manuscript are panels (c-h) discussed? Consider moving panels (c-h) to the supplement and including the MODIS image from Fig. 1d here for an easier comparison.

Response:
Moved MODIS imagery panel from Fig. 1d to old Fig. 9 and moved panels (c-h) to Supplementary. The revised optical depth Fig. 6 is shown below.

Location in revised manuscript: Fig. 14 caption, p. 24, lines 505–515.

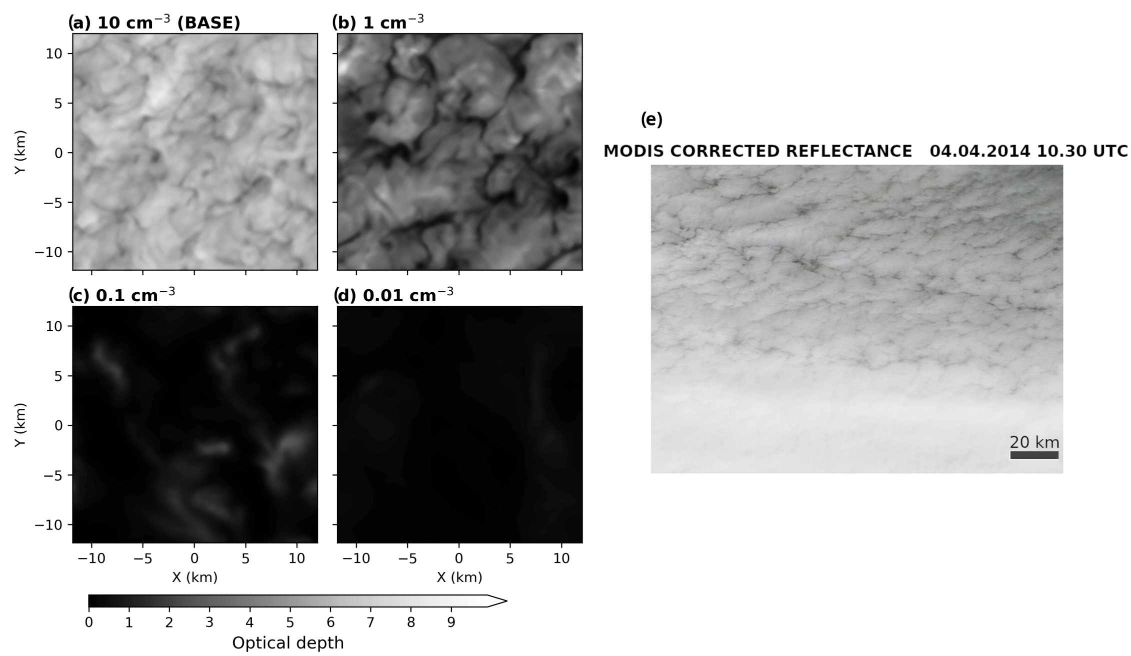

Figure 6: (In revised manuscript Fig. 14) Optical depth for cirrus for varied N_D (a-d) at the last model time step corresponding to 09:00 UTC. Panel (e) shows detailed view of cirrus observed by MODIS at visible spectrum at 10:30 UTC around HALO measured area.

S18. Figure 10: The lines representing DARDAR, MIRA, OPC, Model Base, and NIXE should be assigned unique style markers in addition to color, ensuring the figure remains legible both in greyscale and for readers with color vision deficiencies. Consult the ACP figure submission guidelines in this regard. Clarify whether the lines represent the mean, median or singular values. Which of those lines represent spatially and / or temporally averaged properties? Consider adding the CONV and SEDI lines here as well.

Response:
Thank you for reminder about the ACP guidelines. We have now added the CONV and SEDI lines. All lines represent mean values per altitude bins. Each line has unique line style. In addition, we have modified the Fig. 10 to show data 5–95th percentile ranges. The revised caption is found in Fig. 1 part of response to RC1-G1 which clarifies the nature of the data presented in the figure.

Location in revised manuscript: Fig. 9, p. 17, lines 365–370.

S19. Figure 11: Assign unique style markers to the lines as hey are hard to read with green-red and more severe color vision deficiencies. Add the choice of ND to the panel labels.

Response:
Figure modified accordingly and NDs added to titles. Figure linestyles and markers have been modified additionally to help readability. We have also also 1-σ standard deviation of each bin for both measurements and simulation results. We noticed that panel (a) legend labels were labeled incorrectly and is now corrected. For reference, the modified plot is found below as Fig. 7.

Location in revised manuscript: Fig. 10 caption, p. 19, lines 400–405.

S20. Figure 12: Clarify whether the lines mean, median or singular values and if they are averaged. As mentioned for other figures, consider assigning the lines unique style markers for readability in greyscale.

Response:
Added calculation method to caption of new Fig. 11. The revised caption reads:

Location in revised manuscript: Fig. 12 caption, p. 21, lines 440–445.

"Horizontal mean tendencies of ICNC as a vertical profile at the last time step of the BASE simulation."

S21. Lines 368–374: Could sufficiently high supersaturation for homogeneous freezing be achieved between model output steps, above the observed cloud top (with subsequent sedimentation of the homogeneously formed ice crystals), or as a result of spatial inhomogeneities in the RHi field?

Response:
Model does not suggest that there are sufficiently high RHi in BASE case as you can see in the frequency distribution of RHi in the model domain as shown in the Fig. 5 above. The distribution should contain RHi values closer to 140-150% to have homogeneous freezing occurring. In-situ measurements also found no signal of higher RHi although measurements are only available at 9.5 km altitude which corresponds to the lower part in the cirrus which is also dominated by sedimentation effect suppressing RHi. For clarification, UCLALES-SALSA does not resolve microphysics at sub-grid scales so we do not know unfortunately how RHi variability would look if that was resolved. We have added an explanation of this to the Section 3.1.1 in the following:

Location in revised manuscript: Sect. 3.3.2, pp. 21–22, lines 460–480.

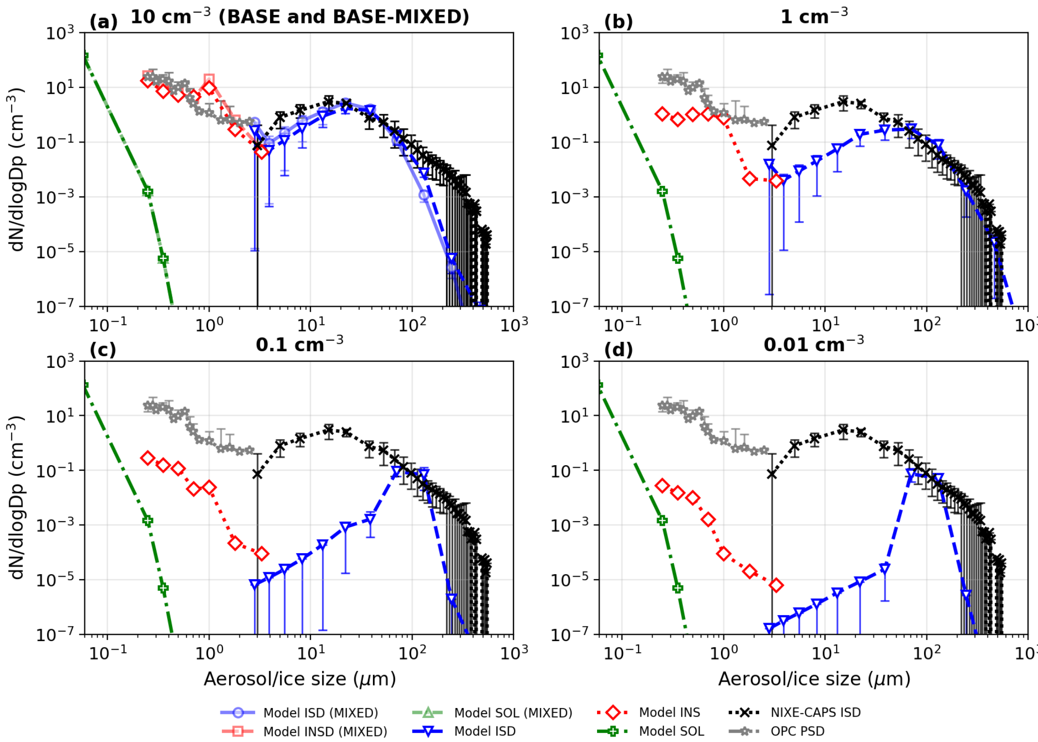

Figure 7: (In revised manuscript Fig. 10) Particle size distributions of SALSA output for varied N_D (10, 1, 0.1 and 0.01 cm^{-3}) (a-d) and NIXE-CAPS measurements. Model level for 9.5 km was used to compare with measurements at constant altitude leg between 09:25 and 09:40 UTC at 9.5 km level inside the cirrus with corresponding temperature $T = 223$ K. The panel (a) represents the BASE and BASE-MIXED simulation PSDs. INS stands for insoluble PSD and SOL for soluble PSD. ISD stands for ice PSD. Error bars represent the 1-σ variability around the mean in each bin.

"A further limitation is that turbulent motions below the LES grid scale are represented through the subgrid-scale closure rather than explicitly solved. Such fluctuations could produce local pockets of RHi that are smoothed within a grid cell, potentially creating conditions favorable for DIN even when the resolved RHi remains close to ice saturation. Kärcher et al. (2025) reported that, for efficient INPs such as mineral dust, turbulent supersaturation fluctuations can promote earlier heterogeneous ice formation, thereby enhancing vapor depletion and reducing subsequent homogeneous freezing. As the LES used in this study does not explicitly resolve subgrid-scale turbulence, its effect on the microphysics cannot be quantified in this study."

S22. Line 378: Clarify or remind the reader on why these range of ND was chosen.

Response:
Part of restructuring of Section 3.4, the sentence was removed.

S23. Line 395: Does the model explicitly distinguish between ice formed by heterogeneous and homogeneous nucleation, or is this inferred from the simulation output?

Response:
Model does explicitly calculate heterogeneous and homogeneous freezing. While the produced ice is the same for both formation mechanisms, diagnostic tracers show the formation rate for both

mechanisms. We added a sentence stating that we do not show homogeneous and immersion freezing rates part of new Fig. 12 because they are at zero:

Location in revised manuscript: Sect. 3.3.2, p. 21, lines 435–445.

"Ice nucleation rates for immersion and homogeneous freezing were not included because they are both at zero."

S24. Section 3.2.1: The first three paragraphs of this section are difficult to follow, as they move rapidly between figures and concepts. The figures in particular have not been sufficiently introduced. Consider restructuring this section to improve clarity and readability.

Response:
Thank you for pointing out. We have restructured these paragraphs so they are easier to follow. Also Fig. 9 was moved as new Fig. 14 with the Fig. 1d panel moved to the Fig. 14 and with removal of vertical wind panels. Now Figures are more closely located to the section which makes it easier to follow the text overall.

Location in revised manuscript: Sect. 3.2, pp. 16–18, lines 335–395; Sect. 3.4, pp. 23–24, lines 485–515.

3.4 Sensitivity to dust number concentration
Figure 10 shows the PSD of aerosols and ice PSD simulated using the H14 scheme compared against in-situ observations at 9.5 km altitude. Mineral dust concentrations ($N_D \approx 10\ \mathrm{cm}^{-3}$) consistent with observations produce ICNC and ice PSD in good agreement with the in-situ measurements at 9.5 km, although ICNC is underestimated below 9 km, as discussed in Sect. 3.2. Under these conditions, DIN dominates ice formation when using the H14 scheme. The continuous production of small ice crystals is sustained, maintaining elevated number concentrations below 50 $\mu\mathrm{m}$ and supporting the observed cloud structure.

As N_D is reduced toward climatological mid-latitude values (Froyd et al., 2022), the ICNC decreases and the mode of the ice PSD shifts toward larger particle sizes. This reduction in N_D leads to insufficient ice production to sustain the observed cloud properties. In particular, for $N_D \leq 0.1\ \mathrm{cm}^{-3}$ cases, the ICNC decreases quickly after the spin up period, indicating that the available INPs are insufficient to sustain the observed ICNC. The reduction in ice production also modifies the thermodynamic and radiative state of the dusty cirrus.
The corresponding IWC response is shown in Fig. 15b. Unlike ICNC, IWC is also constrained by the amount of water vapour available above ice saturation, and its strongest reduction occurs in the cases where the convective structure is lost.
Figure 13 shows the horizontally averaged ICNC and RHi throughout simulations in the N_D within range of $N_D = 0.01 - 10\ \mathrm{cm}^{-3}$. In high N_D simulations, DIN remains sufficiently active to maintain ICNC throughout the simulation. As N_D decreases, heterogeneous ice production weakens, causing ICNC to decline after the spin-up period. At the same time, RHi increases because less ice is available to consume water vapour through depositional growth.
In the lowest $N_D \leq 0.1\ \mathrm{cm}^{-3}$ simulation, the resulting increase in RHi eventually triggers homogeneous freezing, producing initially high ICNC. Thus, homogeneous freezing partially compensates for the reduced heterogeneous ice production, while homogeneous freezing is unable to maintain the convective structure.
Because this compensating contribution from homogeneous freezing is unsustainable, it does not

restore the ICNC required to maintain radiative-dynamical feedback of the dusty cirrus. For $N_D \leq 0.1$ cm^{-3}, the decrease in ICNC weakens LW cooling at the cloud top (Fig. 13). Once SW becomes important during daytime, the weakened LW cooling is no longer sufficient to offset the SW heating. Consequently, the cloud structure transitions from well-defined convective cells to a regime dominated by shear-induced perturbations in vertical velocity, indicating loss of persistence as shown in the Fig. 14. In contrast, for $N_D \geq 1$ cm^{-3}, ice production remains sufficient to sustain convective structure until the end of the simulations. Nevertheless, the morphology of the dusty cirrus depends on N_D. In the $N_D = 10$ cm^{-3} (BASE) simulation, the cloud covered area is relatively homogeneous, with small clear gaps in-between the cells. At $N_D = 1$ cm^{-3}, the cells are more separated with weaker vertical velocity gradient, reflected in reduced ICNC. The organized convective structures simulated for $N_D = 1 - 10$ cm^{-3} are broadly consistent with those observed in the Moderate Resolution Imaging Spectroradiometer (MODIS) (On board TERRA, NASA, 2015) corrected reflectance imagery in Fig. 14e over the model target region and its surroundings. The comparison should nevertheless be interpreted cautiously. The observed cells vary considerable in width and shape, whereas the limited LES domain cannot reproduce the full range of spatial orgnaization. Simulations with a larger horizontal domain would be required to investigate the larger mesoscale structures and spatial variability of dusty cirrus convection.

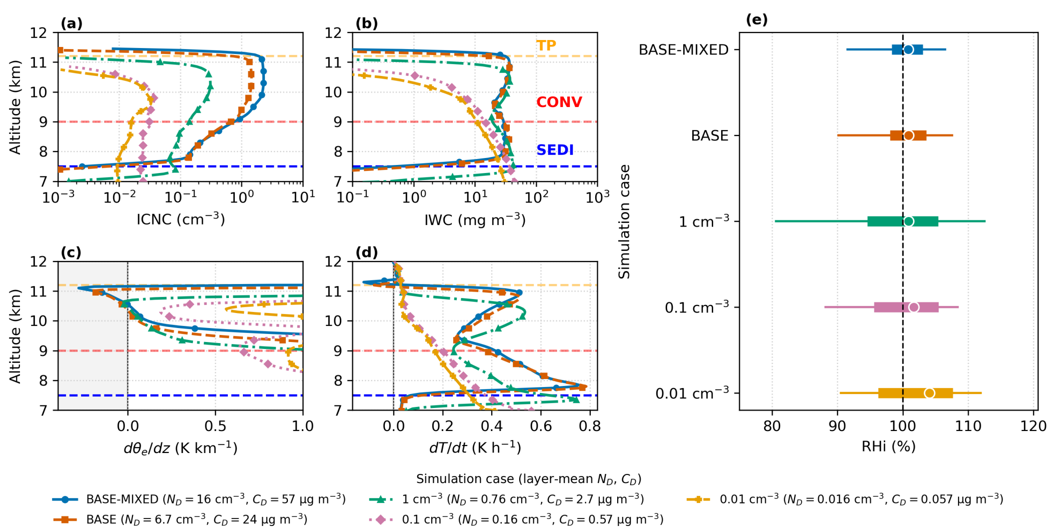

Figure 8: (In revised manuscript Fig. 15) Final-state vertical profiles for the five simulation: (a) ICNC, (b) IWC, (c) vertical gradient of equivalent potential temperature, and (d) net radiative temperature tendency diagnosed from the LW and SW cooling/heating rates. Negative values in panel (c) indicate potentially unstable layers, highlighted in grey; negative values in panel (d) denote net radiative heating/cooling. (e) Distributions of RHi at the final time in the CONV (9 – 11.2 km): horizontal bars span the 5th–95th percentiles, thick lines show the interquartile range, and dots mark the median. The dashed line denotes ice saturation (RHi = 100 %). The N_D values shown in the legend represent the initial layer-mean dust number concentration for each sensitivity simulation, averaged over the CONV-layer levels where dust-induced ice nucleation occurs. The corresponding C_D values represent the initial layer-mean dust mass concentration over the same levels.

The dynamical response is also reflected in the relationship between N_D and atmospheric stability.

The equivalent potential temperature gradient, $\partial\theta_e/\partial z$, shown in Fig. 15c, provides a physically consistent diagnostic for dusty cirrus persistence because it indicates whether the dusty cirrus layer can maintain the instability required for continuous generation of new convective cells and, consequently, new ice crystals. For $N_D \geq 1$ cm^{-3}, negative values of $\partial\theta_e/\partial z$ are found within the CONV layer, indicating that radiative cooling (Fig. 15d) is sufficient to generate conditional instability. For $N_D < 1$ cm^{-3}, $\partial\theta_e/\partial z$ becomes positive, supporting the interpretation presented in Fig. 14 that the generation of new convective cells is no longer sustained. In the borderline case of $N_D = 1$ cm^{-3}, the sufficiently large vertical gradient in temperature tendency (Fig. 15d) can sustain conditional instability despite the absence of strong cooling at the cloud top. Together, these results indicate a threshold of approximately $N_D \approx 1$ cm^{-3} for maintaining the radiative-dynamical feedback and persistent convective structure in the simulated dusty cirrus.

The N_D threshold for sustained convection can be further interpreted in terms of the dust properties that control heterogeneous ice nucleation. Since the INAS-based parameterizations used in this study determine the frozen fraction of particles based on their surface area, the contribution of dust to ice nucleation depends not only on the total number concentration but also on the particle size distribution. Larger dust particles can therefore contribute disproportionately to ICNC even when their number concentration is relatively low. This provides a physical basis for considering dust mass concentration (C_D) in addition to N_D when characterizing the conditions required for persistent dusty cirrus.

Figure 16 shows the predicted INP particle size distribution calculated using the Hiranuma et al. (2014) based DIN activity of mineral dust particles at 218 K for two RHi levels, 105% and 120%. At higher RHi, submicrometer particles dominate the INP population, whereas at lower RHi, the contributions from submicrometer and supermicron particles are more comparable. In contrast, supermicron particles appear relatively insensitive to RHi and activate at similar concentrations under both conditions. As shown in Fig. 15e, RHi values of 120% correspond to the upper range within the model domain, while the standard deviation of RHi is only $\sigma_{\mathrm{RHi}} = 4$–5%. This indicates that conditions closer to RHi = 105% occur more frequently. Consequently, the C_D also provides a useful measure of the potential INP abundance and becomes an important predictor of dusty cirrus persistence.

Figure 8 shows the corresponding C_D values for each N_D simulation. When the simulations are expressed in terms of dust mass concentration rather than number concentration, the transition between sustained and decaying cirrus occurs at approximately $C_D \approx 3$ μg, m^{-3}, integrated over particle diameters $D_p = 0.25$–6 μm. This threshold should be interpreted as a characteristic value for the conditions examined here rather than as a universal threshold, since the relationship between C_D, N_D, and INP activity depends on the dust particle size distribution and the thermodynamic state of the cloud.

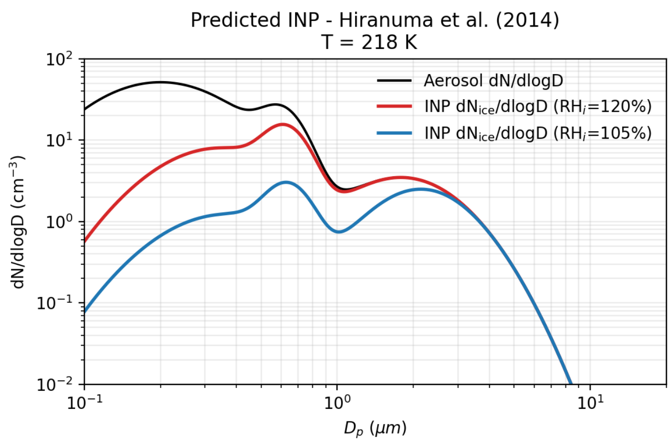

Figure 9: (In revised manuscript Fig. 16) Predicted INP PSD calculated using the Hiranuma et al. (2014) based DIN activity of mineral dust particles shown at fixed temperature and two RHi levels. Black line corresponds to the total fit to the OPC data previously shown in Fig. 16.

S25. Figure 13: Again it is unclear whether these values are averaged. Include the ND values in the panel labels.

Response:
Added calculation method to caption and added ND values. The caption text is shown

Location in revised manuscript: Fig. 13 caption, p. 22, lines 465–470.

"Horizontal means of RHi (shading) and ICNC (contours, cm^{-3}) within the cirrus for different initial N_D in descending order (a)-(d)..."

S26. Figure 14: Clarify if the statistics represent the mean model output and how they are averaged.

Response:
New Fig. 15 was restructured and redesigned (found as Fig. 8 above part of S24) and each statistic presented now is explicitly written in caption. Vertical profiles illustrate better the relationship between mineral dust concentrations and cloud structure vertically and the reader might thus get better idea how stability behaves in SEDI and CONV layer.

Location in revised manuscript: Fig. 15 caption, p. 25, lines 520–525; Sect. 3.4, p. 25, lines 525–530.

S27. Line 409-410: The phrasing of this sentence is confusing.

Response:
Sentence was removed since it did not provide new significant information.

S28. Line 404-410: Is the equivalent potential temperature gradient sufficient to explain the occurrence of new convective cells or are they other dynamical properties that should be considered here?

Response:

We agree that the equivalent potential temperature gradient alone does not describe all aspects of convective-cell formation. However, we have chosen it as an indicator because it is simple to interpret: when positive, the layer is stable and does not support convection, whereas when negative, convection is more easily triggered.

Location in revised manuscript: Sect. 3.4, p. 25, lines 520–530.

S29. Line 416-419: What is the output interval and microphysical timestep of the simulations? Is there are chance that higher RHi values are reached but not recorded as the newly nucleated ice crystals depletes RHi before the next output step?

Response:
The model output interval is 300 s. The model timestep is determined by the Courant–Friedrichs–Lewy condition and is no longer than 1 s. This information has now been added to the model setup description. Also, although the model output interval is much larger than of the ice nucleation scales occurring inside the model domain, if there were any of RHi values close to homogeneous freezing, this would show up within the statistics of the total model domain which covers 24x24 km area. See the discussion regarding Line 368-374 above.

Location in revised manuscript: Sect. 2.4, p. 8, lines 200–207.

"Model time step is determined by the Courant–Friedrichs–Lewy condition but is no longer than 1 s."

S30. Section 3.2.2: This section covers several distinct topics such as sensitivity analysis, the influence of the diurnal cycle, and the representativeness of the case study for regional dusty cirrus. This restuls in rapid transitions between figures and concepts that make the section difficult to follow. Consider splitting this into clearly delineated subsections.

Response:
The sectioning of results was revised and now old Section 3.2.2 (now 3.5) was divided into three subsections "Influence of SW radiation", "Influence of large scale vertical forcing", and "Aerosol direct radiation influence". This hopefully clarifies the overall structure of the manuscript.

Location in revised manuscript: Sect. 3.5, pp. 27–31, lines 550–640.

S31. Line 467-468: Which property is described as stabilizing under SW daytime heating? RHi and ICNC in Figure 16 appear stable in the nighttime scenario and unstable during the day, which seems contrary to the statement made here. Or is this referencing the vertical distribution of net. rad. heating/cooling that promotes some dynamical instability? In that case also elaborate.

Response:
We thank the referee for pointing out this ambiguity. By "stabilization," we refer specifically to atmospheric static stability (stratification), rather than to the temporal stability of RHi or ICNC. Our statement refers to the effect of the vertical distribution of radiative heating and cooling on the thermodynamic stratification of the cloud layer. In particular, the vertical gradient in radiative heating/cooling modifies the vertical gradient of ice-liquid potential temperature and therefore the static stability of the layer. We agree that our original wording was ambiguous and could be interpreted as referring to the temporal variability of RHi or ICNC. We have therefore replaced "stabilization" with "increased/reduced static stability" in each sentence referred to stability. In other places where we refer to instability, we have added "conditional instability" to clarify the nature of instability. Some cases where these changes were applied is shown below:

Location in revised manuscript: Sect. 3.4, p.25, lines 546–550; Sect. 3.5, p. 28, lines 585–595.; Sect. 3.5.1, p. 29, lines 610–615; Sect. 4, p.32, lines 684–690

"Fig. 8c, provides a physically consistent diagnostic for dusty cirrus persistence because it indicates whether the dusty cirrus layer can maintain the conditional instability required for continuous generation of new convective cells and, consequently, new ice crystals." Word used here was just "instability"

"An additional experiment was performed using the aerosol radiation scheme (AERORAD) with the BASE configuration to find whether dust-radiation interaction can have influence on the static stability inside dusty cirrus clouds." was "instability".

"The impacts of SW radiation found in this study are consistent with previous findings that cirrus layers tend to reduce static stability under LW cooling at night and increase static stability under SW heating during daytime (Nagy, 2009; Kollath, 2010)." was "destabilize".

"Longwave radiative cooling weakens the static stability of the cloud layer, thereby supporting convective circulation, whereas shortwave radiative heating counteracts this effect by warming the cloud top during daytime." was "promotes instability".

S32. Line 469-470: Where exactly does the net radiative cooling intensify between 14 and 16 hours? I do not see that in Figure 16.

Response:
Thank you for pointing out. Radiative cooling re-intensification has been highlighted and now should be easily identifiable in new Fig. 17. The modified Fig. 10 is found below with the modified caption:

Location in revised manuscript: Fig. 17 caption, p. 28, lines 580–585; Sect. 3.5.1, p. 28, lines 585–595.

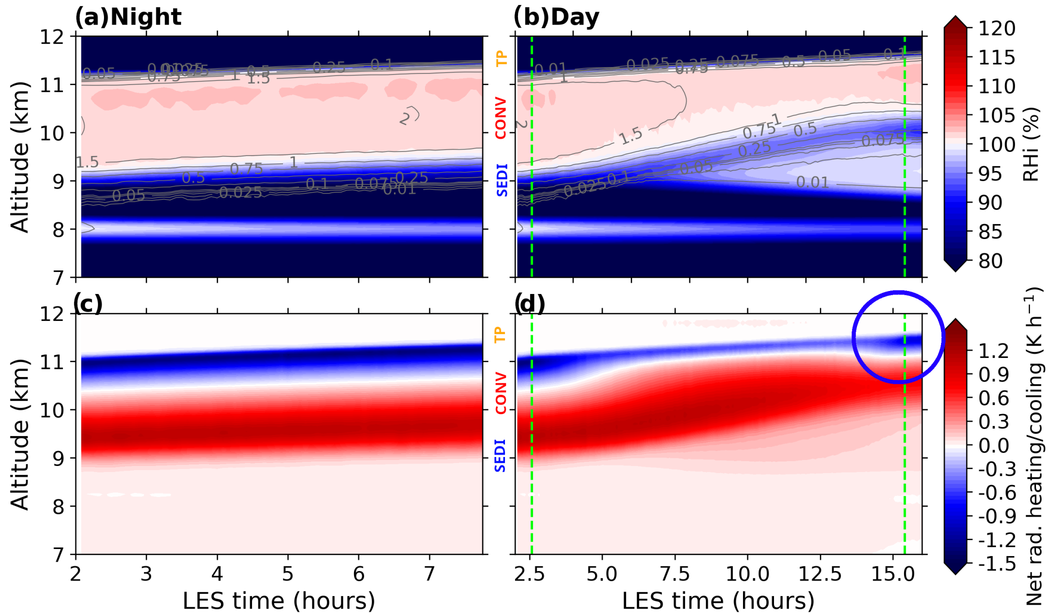

Figure 10: (In revised manuscript Fig. 17) Night (a,c) and daytime (b,d) cases RHi in shading and ICNC (cm^{-3}) in contours in the upper panels. The lower panels show the corresponding net radiative heating/cooling rate. The day case is run for the whole day solar cycle where the downwelling SW radiation at the beginning and at the end of the simulation is close to 0. The vertical dashed line on the left in panels (b) and (d) indicates the time at which solar radiation induces a positive SW flux at the top of the model domain and the second line indicates zero SW flux at sunset. SEDI, CONV, TP have been marked at approximate altitudes since those levels change as dusty cirrus evolves. In panel d), radiative cooling re-intensification has been highlighted with a blue circled area.

S33. Line 475: Figure 18 is referenced before Figure 17. Consider reordering them.

Response:
Reordered. Old Fig. 18 is now still Fig. 18 but old Fig. 17 is now Fig. 19.

Location in revised manuscript: Sects. 3.5.1–3.5.2, pp. 27–30, lines 570–625.

S34. Figure 19: Again, consider assigning the lines unique markers.

Response:
Unique linestyles added to each line. Colors now correspond to LW, SW and net heating rates in

panel (a). Color vision deficiency is take account while selecting the colors. Figure 11 shows the new version below:

Location in revised manuscript: Fig. 20 caption, p. 31

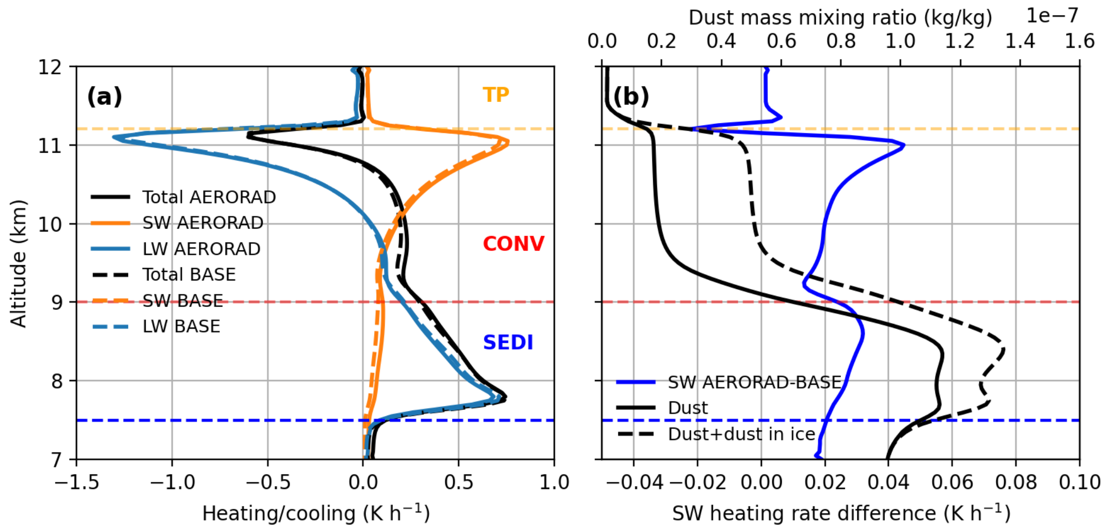

Figure 11: (In revised manuscript Fig. 20) Panel (a) shows aerosol radiation scheme (AERORAD) influence on heating term vertical profile from LW and SW heating rates compared with BASE run using H14 scheme without aerosol radiation. Panel (b) illustrates the SW heating rate absolute difference AERORAD-BASE profile with dust mixing ratio vertical profile.

1.3 Technical Corrections

T1. Equation A2: Explanation of the coefficients and parameters is missing, e.g., wLS.

Response:
We have added definitions of the symbols and parameters, including w_{LS}, in Appendix A, Table A2. The large-scale-forcing term is also identified in the equivalent potential temperature tendency equation in Appendix B.

Location in revised manuscript: Appendix A, p. 36, Table A2; Appendix B, p. 37, lines 720–725.

T2. Figure B1: The second panel has the wrong label.

Response:
Center panel titled Hiranuma et al. (2014) was replaced by Ullrich et al. (2017) in Fig. 12.

Location in revised manuscript: Fig. C1 caption, p. 38, lines 730–735.

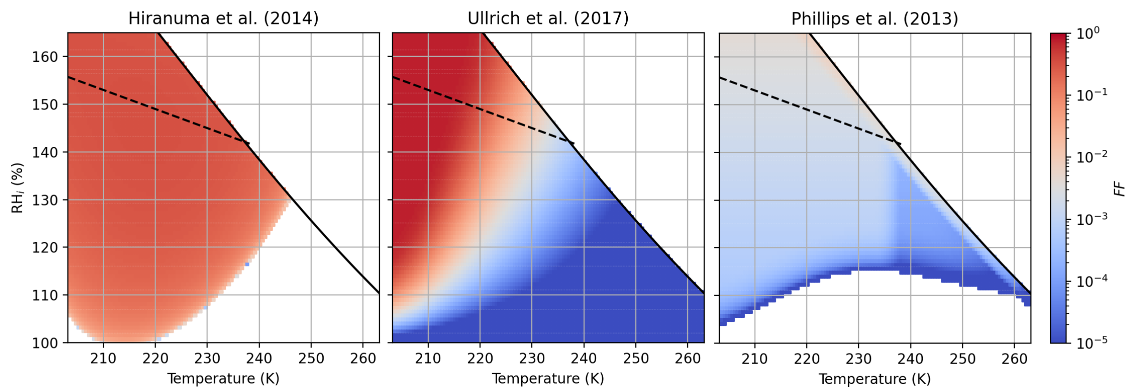

Figure 12: (In revised manuscript Fig. C1) Frozen fraction (FF) calculated based on the aerosol PSD shown in Fig. 16 with Hiranuma et al. (2014, H14), Ullrich et al. (2017, U17) and Phillips et al. (2013, P13) scheme in deposition nucleation conditions. Solid black line indicates water saturation line and the dashed black line Koop et al. (2000) threshold line for onset of homogeneous freezing of aqueous solution droplets.

2 Response to Reviewer 2

Review of "Mineral dust concentration controlling convective cirrus structure and persistence: a large-eddy simulation study with observational constraints" by Juurikkala et al. (2026)

G1. General comments: The work presented in this article offers a deep insight into dusty cirrus clouds by performing large- eddy simulations of one case study. The authors are able to study the evolution of dusty cirrus, the involved microphysical mechanisms and the associated convective dynamics. The results are compared with different satellite products, ground based cloud radar data as well as with in-situ measurements corresponding to the same simulated period. It is a detailed study including sensitivity tests to different initial dust concentrations, different large-scale vertical forcing scenarios and daytime and nighttime simulations. It also compares three schemes for heterogeneous ice nucleation currently available in many models and highlights the need to keep improving this aspect of models. I find it is an interesting study adding valuable information on the nature of dusty cirrus. In general it is well structured, however some paragraphs and figure locations would benefit from a slight reorganization to make the text easier to follow. Some sections could also be improved by adding numerical values that support the conclusions reached with the interpretation of the figures. I consider it is suitable for publication after assessing the following specific and technical comments:

We thank the referee for positive feedback on our manuscript. Please find the responses to specific comments answered below.

2.1 Specific Comments

S1. Since ERA5 is used, I would suggest to add a brief description of the dataset in Section 2 and the following reference: Hersbach, H., Bell, B., Berrisford, P., Hirahara, S., Horányi, A., Muñoz-Sabater, J., Nicolas, J.,

Peubey, C., Radu, R., Schepers, D., Simmons, A., Soci, C., Abdalla, S., Abellan, X., Balsamo, G.,

Bechtold, P., Biavati, G., Bidlot, J., Bonavita, M., De Chiara, G., Dahlgren, P., Dee, D., Diamantakis, M., Dragani, R., Flemming, J., Forbes, R., Fuentes, M., Geer, A., Haimberger, L., Healy, S., Hogan, R. J., Hólm, E. A., Janisková, M., Keeley, S., Laloyaux, P., Lopez, P., Radnoti, G., Rosnay, P. D., Rozum, I., Vamborg, F., Villaume, S., and Thépaut, J.-N.: The ERA5 global reanalysis, Q. J. Roy. Meteorol. Soc., 146, 1999–2049, https://doi.org/10.1002/qj.3803, 2020.

Response:
Added reference and brief description after first mention of ERA5 in Section 2.5 with following:

Location in revised manuscript: Sect. 2.4, p. 10, lines 225–230.

"The spatial and temporal evolution of w_{LS} obtained from hourly ERA5 reanalysis data (Hersbach et al., 2020) is shown in Fig. 1c."

S2. Line 56: which hydrometeors are included in SALSA?

Response:
Added following clarification: "including cloud droplets, drizzle/rain and ice"

Location in revised manuscript: Sect. 2.1, p. 3, lines 60–65.

"The aerosols and hydrometeors including cloud droplets, drizzle/rain and ice in SALSA are described with a sectional bin treatment, a computationally heavy but accurate approach to simulate the aerosol-cloud interactions."

S3. Line 61: which SIP are included in SALSA?

Response:
Added following clarifications and the sentence is now following:

Location in revised manuscript: Sect. 2.1, p. 3, lines 63–67.

"SALSA has undergone several iterations after its implementation in the UCLALES model and now includes atmospheric processes from cloud droplet formation to ice nucleation and several secondary ice production processes including rime splintering, ice-ice collisional break up and droplet shattering (Calderón et al., 2025)."

S4. Line 79: under which conditions do the authors consider it would be important to include the sedimentation and coagulation of aerosols?

Response:
Simulation times in this study are considerably shorter than aerosol settling distances achieved for aerosols smaller than 10 micrometer. In an hour, 2 micrometer aerosols settle only about 25 meters which is only half of a vertical grid. The vertical velocities (vertical wind) inside the dusty cirrus are significantly higher than settling velocities.

Location in revised manuscript: Sect. 2.1, p. 4, lines 85–92; the settling-distance estimate is provided as a response clarification.

S5. Line 86: although it is later shown in Fig. 4a that $T > 210$ K, it could be good to add a sentence after "...temperatures above 210 K." mentioning that this is exactly the case for the presented results.

Response:
We have continued this sentence with the following text:

Location in revised manuscript: Sect. 2.1, p. 4, lines 95–100.

"... and applies to the range of temperatures where the dusty cirrus formed on 4 April."

S6. Line 122: which version of the DARDAR data is being used?

Response:
For DARDAR-Nice, version is 2.1.1 as reported in Sourdeval et al. (2018).

S7. Section 2.4: I personally found this section a little bit messy. Fig 1d is not explicitly mentioned until much later (Section 3.1), Fig. 4 is described before Fig. 3 and Fig. 3 is just mentioned, there is barely no explanation associated with it. Some suggestions are:

Response:
We thank the referee for pointing out. We have clarified terminology and concepts presented within the Section. More detailed response to each point presented below. We provide here the revised Section 2.3:

Location in revised manuscript: Sect. 2.3, pp. 6–8, lines 160–195; Sect. 2.4, pp. 8–12, lines 195–285; Figs. 1–5.

"2.3 Dusty cirrus of 02–05 April 2014
On 2 April 2014, a cut-off low-pressure system developed over the Iberian Peninsula and propagated eastward while intensifying. Along the eastern flank of the system, a developing and strengthening warm conveyor belt (WCB) leading a cold front produced high surface winds and resulted in high emissions of mineral dust over the northern Sahara around the Atlas Mountains and the Moroccan-Algeria border that were transported by the WCB to higher in troposphere (Weger et al., 2018). MSG Seviri IR satellite imagery (not shown) on 3 April reveals an extensive region of dusty cirrus associated with convective cells embedded within the WCB outflow and by 4 April the dust was transported over a large area over Europe which was identifiable as a large shield of cirrus. As part of the ML-CIRRUS campaign, research flights using HALO were conducted to sample these clouds. On 4 April, the aircraft intercepted and directly measured the extensive cirrus layer as shown in Fig. 1 a, b.
Figure 2 shows the vertical profile of measured concentrations of aerosols and ice below 9.5 km. Above 7 km, the OPC measured elevated concentrations of aerosols for total number and filtered for sizes above 500 nm showing that the Saharan dust plume had still quite high concentrations of large dust particles. Roughly at 8 km, HALO encountered near supersaturated conditions over ice with high ICNC values that were most likely connected to the elevated presence of dust (Weger et al., 2018).
The sounding measured at Innsbruck Airport, Austria, at 03:00 UTC on 4 April (Fig. 3a, black solid line) indicates a layer of weak static stability between 9 and 11 km, where the vertical gradient of potential temperature ($\partial\theta/\partial z$) is small. Panel a) shows temperature and potential temperature. Equivalent potential temperature (θ_e) was calculated from the sounding profile of θ using Eq. **??**, *and its vertical gradient was used as a diagnostic of potential instability under large-scale forcing. Between 9 and 11 km, the calculated gradient ($\partial\theta_e/\partial z$) is negative (not shown), indicating a potentially unstable layer in which latent heating associated with ice–vapor phase changes may support the development of convective cells. The horizontal wind velocity profile shown in Fig. 13c indicates*

weak vertical shear within this layer, with $\frac{du}{dz} \approx 2 \times 10^{-3}\ s^{-1}$. The gradient Richardson number is well above the critical value ($Ri \gg 0.25$), suggesting that shear-induced instability is unlikely to dominate and that the observed instability is primarily thermodynamic. Recently, Pieper et al. (2026) found that vertical wind shear is not a significant contributor whether dusty cirrus related turbulence occurs or not, thus we can rule out that vertical wind shear might influence the outcome of this study significantly. The sounding evidence for an unstable layer between 9 and 11 km is supported by the presence of organized up- and downdrafts in the MIRA-35C Doppler velocity observations at Schneefernerhaus (approx. 50 km from Innsbruck) during the early hours of 4 April (Fig. 4b). We define the convective layer as CONV as highlighted with blue dash lines in Fig. 3 panels a and b. Figure 4a shows that high IWC is found throughout the turbulent CONV layer. Intense updrafts prevent large ice crystals from precipitating out of the cloud and allows them to continue growing even further. On the other hand, a layer between 7 and 9 km (Fig. 3a) is moderately stable and cirrus at this level is forming from the influence of large-scale vertical velocity and from ice crystals sedimenting from the CONV layer. For this reason, we refer to this layer as SEDI as shown in Fig. 3 panels a and b."

S7a. in line 159: "... under large scale lifting as shown in Fig.1." Specify in which panel (panel d?)

Response:
Reference to Fig. 1 was removed since it was misleading reference to a figure. Figure 1d panel was also moved to new Fig. 14 panel e. See the Fig. 6 part of response to RC1 S19.

Location in revised manuscript: Fig. 14 caption, p. 24, lines 505–515.

S7b. Line 158 – 161: I would suggest rewriting this part to make clear that the sounding profiles in Fig. 4a correspond to T and θ and not to θ_e and that θ_e and its gradient are computed but not shown.

Response:
We have modified the text in this part to make it clearer that the plot shows θ instead of θ_e by modifying it in following way:

Location in revised manuscript: Sect. 2.3, pp. 7–8, lines 175–190.

"Equivalent potential temperature (θ_e) was calculated from the sounding profile of θ using Eq. B2, and its vertical gradient was used as a diagnostic of potential instability under large-scale forcing. Between 9 and 11 km, the calculated gradient ($\partial\theta_e/\partial z$) is negative (not shown), indicating a potentially unstable layer in which latent heating associated with ice–vapor phase changes may support the development of convective cells."

S7c. Line 161: specify where do we find the horizontal wind velocity profile (Fig. 4c?)

Response:
Added reference to Fig. 3c (was Fig. 4c). Text was modified in the following way:

Location in revised manuscript: Sect. 2.3, p. 8, lines 180–190.

"The horizontal wind velocity profile shown in Fig. 3c indicates weak vertical shear within this layer, with $\frac{du}{dz} \approx 2 \times 10^{-3}\ s^{-1}$."

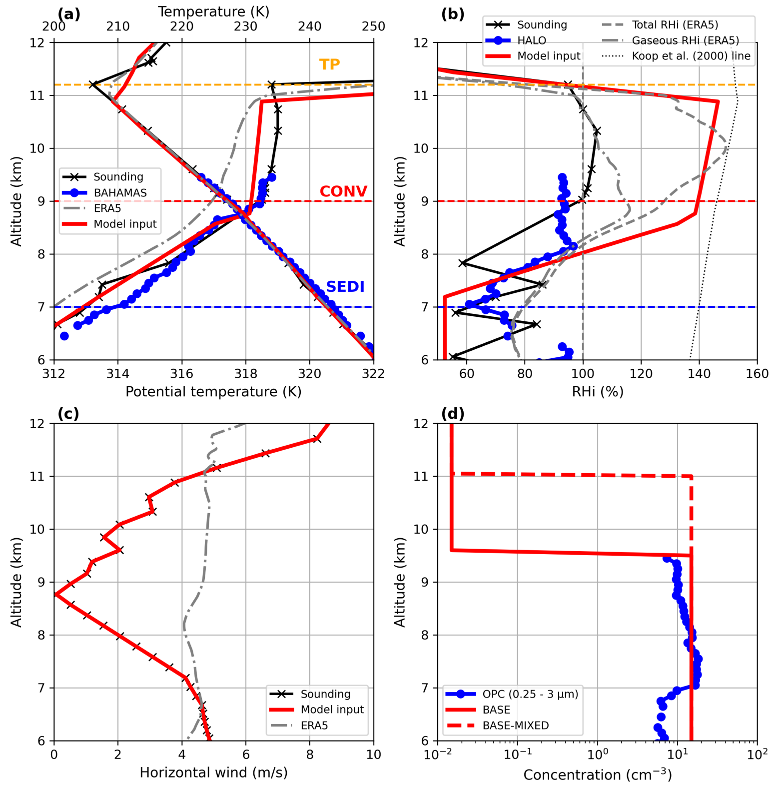

Figure 13: (In revised manuscript Fig. 3) Initial vertical profiles used in the UCLALES-SALSA simulations and corresponding observations. Panel (a) shows potential temperature (lower x-axis) and temperature (upper x-axis), panel (b) shows RHi, panel (c) shows horizontal wind speed, and panel (d) shows aerosol number concentration. In panels (a) and (b), black, blue and red lines denote the sounding, BAHAMAS measurements, and model input, respectively. Grey lines show ERA5 values at the initial point of the 6 hour LAGRANTO trajectory. In panel (b), dash dot and dashed grey lines denote vapor phase and total RHi (vapor phase and ice phase water) respectively. The dotted line in panel (b) indicates the homogeneus freezing threshold corresponding to Koop et al. (2000) (equation from Ren and Mackenzie (2005)). In panel (c), red and grey lines show the prescribed wind profile and ERA5 wind, respectively. In panel (d), the blue line shows the OPC aerosol concentration for particles between 0.25 and 3 μm, while the solid and dashed red lines show the BASE and BASE-MIXED dust profiles. The CONV and SEDI layers are marked by red and blue horizontal lines, respectively, and the tropopause (TP) is indicated by an orange line.

S7d. I think Fig. 3a is not used. I would suggest merging Fig. 3a with Fig. 3b by having the color code of w and IWC contours on top to identify the cloud.

Response:

A sentence using Fig. 3a was modified. We appreciate the suggestion of combining panels, however, we have kept the figure in the original form to retain easy readability.

Location in revised manuscript: Sect. 3.1, pp. 13–14, lines 295–305.

"Figure 4a shows that high IWC is found throughout the turbulent CONV layer. Intense updrafts prevent large ice crystals from precipitating out of the cloud and allows them to continue growing even further."

S7e. If the authors believe it would improve the readability, perhaps Fig. 4 could be placed before Fig. 3.

Response:
Ordering was changed as suggested.

Location in revised manuscript: Figs. 2–4, pp. 7–10, and Sect. 2.3, pp. 7–8, lines 165–195.

S7f. Caption of Fig. 4: I would suggest explicitly describe what is seen in each panel, as it is done in the rest of figures.

Response:
Thank you for your suggestion. We have written out everything on the current Fig. 3 (previously Fig. 4) explicitly now. See the revised caption in Fig. 13 above.

Location in revised manuscript: Fig. 3 caption, p. 9, lines 210–215.

S8. Line 179: the model top is at 14 km, out of curiosity, how thick is and at what altitude does the sponge layer start in the used set-ups?

Response:
The sponge layer starts around 12.8 km, around 1.5 km above the cloud tops. The sponge layer was located at top 5 model levels. At those levels, tropopause inversion made the layer stable. We have now specified that LES has Newtonian relaxation points (sponge layer) at the model top as follows:

Location in revised manuscript: Sect. 2.1, p. 3, lines 55–62.

"Model top contains a sponge layer with adjustable number of Newton relaxation points."

S9. Line 186: what humidity profile is modified? The sounding? Can the authors explain a bit more how the modifications were done, which decisions were taken?

Response:
Sounding was modified to initialize model convection more naturally. The higher RHi was used because dust particles are initially dry and water vapor deposition onto ice reduces RHi close to 100 % quickly after onset of ice nucleation. Latent heating related to this is accounted for by using a lower initial potential temperature. We have added this text following the introduction of humidity profile set up:

Location in revised manuscript: Sect. 2.4, pp. 9–10, lines 210–220.

"The higher RHi is used because dust particles are initially dry and water vapor deposition onto ice reduces RHi close to ice saturation quickly after the onset of ice nucleation."

S10. Line 191: to which line in Fig. 4b corresponds the integrated RHi profile? Is it the solid blue line?

Response:
This sentence was written confusingly. We meant that the integrated water vapor content in the layer between 8.5-11 km corresponds roughly to ice water content added to background water vapor content measured at 9.5 km in altitude. Modified followingly:

Location in revised manuscript: Sect. 2.4, p. 10, lines 215–225.

"The initial RHi profile corresponds to total water content (vapor as measured with BAHAMAS combined with NIXE-CAPS IWC) inside the dusty cirrus."

S11. Line 239: the authors specify that the BASE and sensitivity runs are simulated using H14. Is this also the case for BASE-MIXED?

Response:
BASE-MIXED cases are simulated alongside the BASE in mode–observation comparison and in the varied N_D simulations. In the sensitivity runs BASE-MIXED is not used. The text is clarified in text as following:

Location in revised manuscript: Sect. 2.4, p. 12, lines 260–275.

"The BASE case and all sensitivity simulations involving radiation and large-scale forcing use H14 as the default DIN parameterization. To assess the sensitivity to the choice of DIN parameterization, we additionally perform simulations using the BASE configuration with two alternative schemes, U17 and P13. The BASE-MIXED configuration is used alongside BASE in the model–observation comparison and in the N_D sensitivity simulations."

S12. Line 258: "recycled ice crystals" what do the authors mean by this term?

Response:
We replaced this sentence to have following form:

Location in revised manuscript: Sect. 3.1, pp. 13–14, lines 295–305.

"Sublimation releases mineral dust particles that previously nucleated ice, allowing them to participate again in ice formation when re-entrained into updrafts."

S13. Figure 9 is presented in Section 3.1 but is barely explained. If the authors agree, Fig. 9 and the paragraph from line 297-300 could be moved to Section 3.2.1

Response:
Thank you for suggestion. We have moved the old Fig. 9 to under new Section 3.4 (corresponding to old Sect. 3.2.1). The old version of the figure was moved to Supplements and updated figure has only optical depth panels with panel from old Fig. 1d added as panel (e). Please find the modified Fig. 6 under response to RC1-S17.

Location in revised manuscript: Sect. 3.4, pp. 23–24, lines 485–515, and Fig. 14 caption on p. 24.

S14. Section 3.1.1 could benefit of the addition of numerical values in the explanations, especially for IWC. For example, in how many order of magnitudes the values differ, means, variability, etc.

Response:
Thank you for a good suggestion. We have added a supporting table below old Fig. 10 (now Fig. 9) which can be followed while reading the old Section 3.1.1 (now 3.2). Additionally we have

added numerical values in the explanations, both for IWC and ICNC. The modified Section is now modified as follows:

Location in revised manuscript: Sect. 3.2, pp. 16–18, lines 335–380; Table 1 on p. 16.

"We compare the model performance at the end of the BASE and BASE-MIXED simulations, corresponding to 09:00 UTC when HALO measured the dusty cirrus layer. Table 3 summarizes the representative values and variability shown in Fig. 9. The modeled IWC vertical profile generally agrees with the range of in-situ measurements, although the modeled mean IWC in the CONV layer is approximately 30% *higher than the NIXE-CAPS mean. The difference between BASE and BASE-MIXED is only about* 0.7% *in the CONV layer, indicating very similar modeled IWC values. The DARDAR-Nice profiles obtained during the noon overpass show mean IWC values of* $19.22 \pm 10.85\ \mathrm{mg\,m^{-3}}$ *and* $16.77 \pm 8.40\ \mathrm{mg\,m^{-3}}$ *in the CONV and SEDI layers, respectively. The DARDAR-Nice estimates cover a larger horizontal area and therefore sample a broader range of cirrus conditions, with IWC values varying by approximately one order of magnitude, while their mean values remain within the same order of magnitude as the modeled values. MIRA-35C IWC is lower than both NIXE-CAPS and DARDAR-Nice, with a mean value of* $9.03 \pm 5.93\ \mathrm{mg\,m^{-3}}$ *in CONV, approximately* 60% *lower than NIXE-CAPS and* 53% *lower than DARDAR-Nice. However, the upper range of MIRA-35C estimates approaches the modeled IWC values. MIRA-35C also observes cirrus conditions at a larger scale, similar to DARDAR-Nice, since the statistics represent a couple of hours of dusty cirrus flowing over the radar station. The common feature in the modeled and observed cirrus is the shape of the IWC profile between 9 and 11.5 km (CONV), where IWC increases towards the cloud top. While IWC was not sampled above 9.5 km with NIXE-CAPS, the IWC agrees well within the sampled altitude range.*

For ICNC, the vertical profile has a very similar shape to the IWC profile in the CONV layer for both BASE and BASE-MIXED cases. The modeled ICNC varies within a range comparable to that observed by NIXE-CAPS, although the NIXE-CAPS mean ICNC is approximately $1.9\times$ *and* $1.2\times$ *higher than the BASE and BASE-MIXED means, respectively. The comparison of mean ICNC between the model and NIXE-CAPS is, however, subject to sampling uncertainty because NIXE-CAPS covers only approximately 500 m of the CONV layer, while the agreement is good at the uppermost altitude sampled by the measurements. In the SEDI layer, the mean NIXE-CAPS ICNC is* $1.87\ \mathrm{cm^{-3}}$*, compared with* $0.24\ \mathrm{cm^{-3}}$ *and* $0.25\ \mathrm{cm^{-3}}$ *for BASE and BASE-MIXED, respectively. Thus, the observed mean is approximately* $7.8\times$ *and* $7.5\times$ *higher than the modeled means, and the NIXE-CAPS ICNC values exceed the full range simulated within the LES domain. The HALO aircraft had a horizontal footprint of approximately 23–24 km during the ascent between 8 and 8.8 km altitude with a true air speed of roughly 190* $\mathrm{m\,s^{-1}}$*, corresponding to approximately 190 m horizontal sampling resolution for NIXE-CAPS. This is comparable to the LES model domain horizontal extent of 24 km and its 150 m horizontal resolution. The lack of similarly high ICNC values in the model and NIXE-CAPS measurements within the SEDI layer suggests that processes in the model setup or microphysical treatment may contribute to the difference. This is discussed further in Sect. 3.3.*

DARDAR-Nice estimates of ICNC for ice particles with $D_i > 5\ \mu\mathrm{m}$ *show a very similar vertical profile to the model results. In the CONV layer, however, the DARDAR-Nice mean ICNC of* $0.62 \pm 0.42\ \mathrm{cm^{-3}}$ *is approximately* 50% *lower than the BASE mean and* 68% *lower than the BASE-MIXED mean. Its variability is nevertheless substantial, with a standard deviation of* $0.42\ \mathrm{cm^{-3}}$*, exceeding that of BASE at* $0.22\ \mathrm{cm^{-3}}$ *and being comparable to that of BASE-MIXED at* $0.31\ \mathrm{cm^{-3}}$*. In the SEDI layer, the DARDAR-Nice mean of* $0.23 \pm 0.15\ \mathrm{cm^{-3}}$ *is close to the modeled means* *of* $0.24 \pm 0.04\ \mathrm{cm}^{-3}$ *for BASE and* $0.25 \pm 0.04\ \mathrm{cm}^{-3}$ *for BASE-MIXED. To ensure comparability between the model, NIXE-CAPS, and DARDAR-Nice, we also calculated ICNC for ice particles larger than* $5\ \mu\mathrm{m}$ *for both NIXE-CAPS and the model. This resulted in only marginal changes to ICNC, suggesting that the DARDAR-Nice estimates should be representative of the total ICNC. Although the DARDAR-Nice and model ICNC profiles agree reasonably well, the larger NIXE-CAPS ICNC values in the SEDI layer cannot be uniquely attributed to model processes. The model is forced along a single ERA5-derived trajectory between 03:00–09:00 UTC, while DARDAR-Nice provides observations from the 12:30 UTC CloudSat overpass. The final model state was selected to have a thermodynamic state comparable to that observed during the CloudSat overpass, providing a useful basis for comparison, but the difference in sampling time means that the observations and model do not necessarily represent the same stage of cloud evolution. These differences should therefore be considered when interpreting the agreement and discrepancies between the model and observational datasets."*

S15. Line 344: it is mentioned that the differences between the ICNC produced by the different DIN schemes come from differences in the T and RHi dependencies of the parameterizations at $T < 210$ K. However, it seems that for the studied dusty cirrus $T < 210$ K for most of the layer. Could the authors elaborate on this?

Response:
Corrected to "below 230K". Also the Fig. B1 (now C1) has wrong title for middle panel, which has been corrected to Ullrich et al. (2017). Also units have been changed from Celsius to Kelvin. Corrected sentence is:

Location in revised manuscript: Sect. 3.3.1, p. 19, lines 405–415; Fig. C1 caption, p. 38.

"These differences originate from the distinct temperature and RHi dependencies of the parameterizations at temperatures below 230 K."

S16. Line 403: could the authors expand on the behavior of IWC to ND as it was done for ICNC?

Response:
Extended the existing sentence about the IWC as:

Location in revised manuscript: Sect. 3.4, p. 23, lines 490–500; Fig. 15 caption, p. 25, lines 520–525.

"The corresponding IWC response is shown in Fig. 15b. Unlike ICNC, IWC is also constrained by the amount of water vapour available above ice saturation, and its strongest reduction occurs in the cases where the convective structure is lost."

S17. Line 411-426: I think the flow in Section 3.2.1 would be improved if these paragraphs are moved after line 403, since there is continuation in the analysis of the ICNC.

Response:
We thank the referee for this suggestion. We carefully reconsidered the ordering of these paragraphs and revised the discussion to improve the continuity of the analysis. We retained the discussion of the N_D–stability relationship before the INAS-based analysis because the stability analysis establishes the threshold in N_D for sustaining the radiative-dynamical feedback and persistent convection. The subsequent INAS discussion then provides a microphysical interpretation of this threshold by relating it to the dust particle size distribution and dust mass concentration C_D. In this ordering, the C_D threshold is introduced as a consequence of the identified N_D threshold rather than before the dynamical criterion has been established. We believe this provides a clearer progression from the ICNC response to its dynamical consequences and finally to the microphysical interpretation of the threshold for sustained dusty cirrus convection.

Location in revised manuscript: Sect. 3.4, pp. 23–26, lines 485–550.

S18. In Section 3.2.2, Fig. 18 is discussed before Fig. 17. I would suggest either rearranging the figures or the paragraph order.

Response:
The ordering was changed as suggested.

Location in revised manuscript: Sects. 3.5.1–3.5.2, pp. 28–30, lines 585–625.

T1. Technical comments: Please, review the format of the dates and choose one for consistency. In some cases it is written April 3th or April 4rd and in others 4 April.

Response:
We have reviewed the ACP guidelines regarding the dates and times. We have thus updated dates in each location for example as 4 April. Time format has been changed to 12:00 UTC.

Location in revised manuscript: pp. 3–33; date and time expressions were standardized at the locations listed below.

T2. Please, review the use of articles and the punctuation.

Response:
We have checked the use of articles and punctuation. We also thank the referee for the suggested corrections below.

Location in revised manuscript: throughout pp. 1–41; copy-editing changes were distributed throughout the manuscript.

T3. Line 111: there is an extra space in "(35…"

Response:
Modified as suggested.

Location in revised manuscript: Sect. 2.2.2, p. 5, lines 130–140.

T4. Line 142 - 143: "… over northern Sahara around Atlas Mountains and Moroccan-Algeria border..." – "...over the northern Sahara around the Atlas Mountains and the Moroccan-Algerian border…"

Response:
Modified as suggested.

Location in revised manuscript: Sect. 2.3, p. 6, lines 160–165.

T5. Line 143: "… by WCB to higher in troposphere..." – "… by the WCB higher into the troposphere"

Response:
Modified as suggested.

Location in revised manuscript: Sect. 2.3, p. 7, lines 160–170.

T6. Line 144: "..satellite imagery (not shown) on April 3rd reveal…" – "...satellite imagery (not shown) on April 3rd reveals…"

Response:
Modified as suggested.

Location in revised manuscript: Sect. 2.3, p. 7, lines 160–170.

T7. Line 146: "..was identifiable as large shield..." – "...was identifiable as a large shield…"

Response:
Modified as suggested.

Location in revised manuscript: Sect. 2.3, p. 7, lines 165–170.

T8. Figure 1:

T8a. at the bottom, between panels c) and d) it is written "HALO measurements". Is this suppose to be there? Yes but the placement is confusing. This will be highlighted better.

Response:
We removed the HALO measurements since it was confusing here. Please find the modified Figure below as Fig. 14.

T8b. there is a grey line right of panel d)

Response:
Panel 1d was moved to new Fig 14 panel e) and the grey line was removed.

Location in revised manuscript: Fig. 14 caption, p. 24, lines 505–515.

T8c. it could be useful to add in the caption that the color lines in panel a) and b) correspond to the HALO flight track with color code altitude in km.

Response:
Added explanation of HALO flight track to caption with following text:

Location in revised manuscript: Fig. 1 caption, p. 6, lines 155–160.

"(a) MSG IR 8.7 µm *channel imagery over Europe with HALO flight track altitude marked with colored line corresponding to altitude with (b) zoomed view with LAGRANTO 6 hour parcel trajectory (black solid line) and observation points marked with red dot. Panel (c) shows the vertical velocity from ERA5 along the parcel trajectory shown in (b)."*

T9. Line 152: "." missing at the end of the sentence.

Response:
Modified as suggested.

Location in revised manuscript: Sect. 2.3, p. 7, lines 160–170.

T10. Line 155: "Sounding profile measured…" – "The sounding profile measured…"

Response:
Modified as suggested.

Location in revised manuscript: Sect. 2.3, pp. 7–8, lines 175–185.

T11. Line 158: "Vertical gradient of…" – "The vertical gradient of…"

Response:
Modified as suggested.

Location in revised manuscript: Sect. 2.3, p. 8, lines 175–185.

T12. Line 158-159: "...leads to new development…" – "leads to the new development"

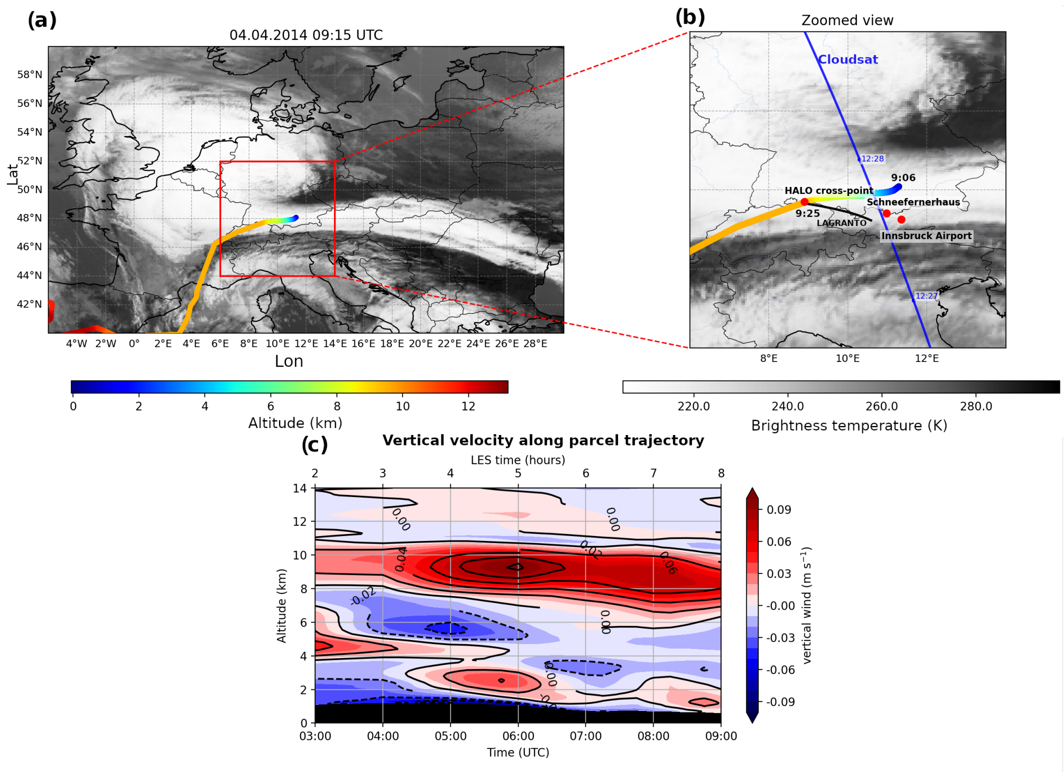

Figure 14: (a) MSG IR 8.7 μm channel imagery over Europe with HALO flight track altitude marked with colored line corresponding to altitude with (b) zoomed view with LAGRANTO 6 hour parcel trajectory (black solid line) and observation points marked with red dot. Panel (c) shows the vertical velocity from ERA5 along the parcel trajectory shown in (b).

Response:
Modified as suggested.

Location in revised manuscript: Sect. 2.3, p. 8, lines 175–185.

T13. Line 160: "... find potentially unstable layer ..." – "... find a potentially unstable layer..."

Response:
Modified as suggested.

Location in revised manuscript: Sect. 2.3, p. 8, lines 175–185.

T14. Line 165: "...early hours of April 4 (Fig. 3)" – "...early hours of April 4 (Fig. 3b)" (If suggestion of merging panel a and b is not followed).

Response:
Modified as suggested.

Location in revised manuscript: Sect. 2.3, p. 8, lines 185–195.

T15. Line 166 and line 170: I think it was meant "as shown in Fig. 4 panels a and b" instead of Fig. 3

Response:
Modified as suggested.

Location in revised manuscript: Sect. 2.3, p. 8, lines 185–195.

T16. Figure 2:

Response:
Modified as suggested.

T16a. Caption: "... marked with black vertical line..." – "... marked with a black vertical line"

T16b. I think in the legend the dashed-dot line should be dashed to match the plot.

Response:
Legend handles were fixed to match with the lines on the plot. Figure found below as Fig. 15.

Location in revised manuscript: Fig. 2 caption, p. 7.

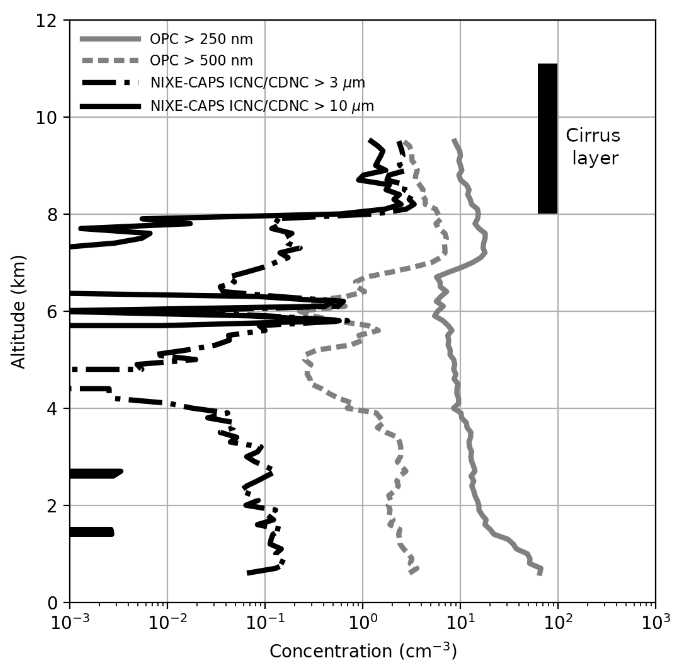

Figure 15: (In revised manuscript Fig. 2) Vertical profile of NIXE-CAPS and OPC measured concentrations of ice and aerosols respectively during the HALO vertical ascent up to 9.5 km between 09:22-09:25 UTC. Extent of cirrus layer is marked with a black vertical line between 8-11 km.

T17. Line 182-184: "the model domain follows solar diurnal cycle at latitude 47.5° and therefore experiences both nighttime conditions in the initial 2.5 hours and daytime conditions for the latter half of the simulation time." – " the model domain follows the solar diurnal cycle at latitude

47.5° and therefore experiences both nighttime conditions during the initial 2.5 hours and daytime conditions during the latter half of the simulation time.”

Response:
Modified as suggested.

Location in revised manuscript: Sect. 2.4, p. 8, lines 200–207.

T18. Line 186: “The sounding profile is used. . . ” – “The sounding profile (Fig. 4a, also b?) is used. . . ”

Response:
Modified as suggested.

Location in revised manuscript: Sect. 2.4, p. 8, lines 210–215.

T19. Line 188: “between 8.5 and 10.8 km (as shown in Fig. 4)” – “between 8.5 and 10.8 km (as shown in Fig. 4b) ”

Response:
Modified as suggested.

Location in revised manuscript: Sect. 2.4, p. 8, lines 210–220.

T20. Line 188-189: “. . . profile line in Fig. 4. . . ” – “. . . profile line in Fig. 4B”

Response:
Modified as suggested.

Location in revised manuscript: Sect. 2.4, p. 8, lines 210–220.

T21. Line 192: “. . . the model input potential profile between. . . ” – “. . . the model input potential temperature between . . . ” ?

Response:
Modified as suggested.

Location in revised manuscript: Sect. 2.4, p. 10, lines 215–225.

T22. Line 192: “. . . is set at fixes gradient. . . ” – “. . . is set at a fixed gradient. . . ”

Response:
Modified as suggested.

Location in revised manuscript: Sect. 2.4, p. 10, lines 215–225.

T23. Line 203: please, explain what w_{LS}:

Response:
Modified as suggested. Brief explanation of w_{LS} added in the following:

Location in revised manuscript: Sect. 2.4, p. 10, lines 225–230.

“..., we apply large scale vertical velocity (w_{LS}) forcing to the model domain.”

T24. Line 206: “...in altitude compared to sounding RHi 6 hours prior (Fig. 4).” – “...in altitude compared to the sounding of RHi 6 hours prior (Fig. 4b).”

Response:
Modified as suggested.

Location in revised manuscript: Sect. 2.4, p. 10, lines 230–235.

T25. Line 207: "Satellite imagery (Fig. 1) shows that the cirrus..." – "Satellite imagery (Fig. 1a, b) shows that the cirrus. . . "

Response:
Modified as suggested.

Location in revised manuscript: Sect. 2.4, pp. 10–11, lines 230–245.

T26. Figure 5: would it be possible to plot the total fit in front of the red line? It is difficult to see.

Response:
Thank you for suggesting. The Figure 5 was redesigned to enhance readability overall and it is shown in Fig. 16.

Location in revised manuscript: Fig. 5 caption, p. 11, lines 250–255.

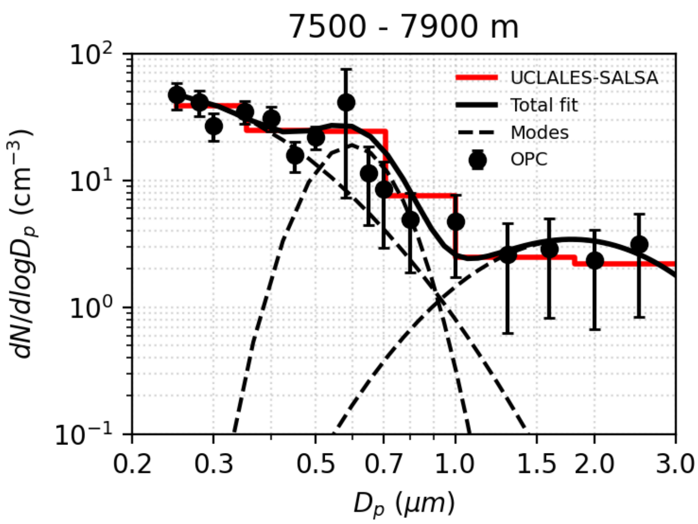

Figure 16: (In revised manuscript Fig. 5) Aerosol size distribution measured by the OPC immediately below the dusty cirrus cloud layer at altitudes between 7.5 and 7.9 km. Black markers indicate the mean measured aerosol number concentration, with vertical error bars representing the standard deviation. The measured distribution was fitted with three lognormal modes, whose sum is shown by the black solid line. The individual fitted modes are shown by the dashed black lines and were used to describe the aerosol size distribution in SALSA. The red solid line shows the dust size distribution used in the UCLALES-SALSA simulations, obtained from the fitted lognormal modes. The fitted mode parameters are: $D_1 = 0.2$ μm, $\sigma_1 = 1.75$, $N_1 = 31.4$ cm^{-3}; $D_2 = 0.6$ μm, $\sigma_2 = 1.2$, $N_2 = 3.8$ cm^{-3}; and $D_3 = 1.8$ μm, $\sigma_3 = 1.57$, $N_3 = 1.7$ cm^{-3}.

T27. Line 226: ". . . PSD which makes this extrapolation justified." – ". . . PSD which justifies this extrapolation."

Response:
Modified as suggested.

Location in revised manuscript: Sect. 2.4, p. 12, lines 255–265.

T28. Line 228: ND was already defined in line 45 as "mineral dust number concentration".

Response:
Modified as suggested.

Location in revised manuscript: Sect. 2.4, p. 12, lines 255–265.

T29. Line 229: "was extended up to 11 km." – "was extended up to 11 km (Fig. 4d)."

Response:
Modified as suggested.

Location in revised manuscript: Sect. 2.4, p. 12, lines 260–270.

T30. Line 235: " ...for upper troposphere Minikin et al. (2003)." – "... for upper troposphere by Minikin et al. (2003)" ?

Response:
Modified as suggested. We changed the reference as bracketed.

Location in revised manuscript: Sect. 2.4, p. 12, lines 270–275.

T31. Line 249: " using H14. U17 and P13 are used to assess sensitivity of ice nucleation pathways..." – " .... using H14, U17 and P13 to assess the sensitivity of ice nucleation pathways..."

Response:
The sentence should end here between H14 and U17 since H14 is used in the simulation results for Sections 3.1–3.2 while U17 and P13 are used as additional schemes used for Section 3.3.

Location in revised manuscript: Sect. 2.4, p. 12, lines 275–280.

T32. Caption Fig. 6: please specify that the contours in the upper panels correspond to RHi.

Response:
We have added the specification of RHi to the caption:

Location in revised manuscript: Fig. 6 caption, p. 13, lines 295–300.

"Black contours in (a-d) represent RHi at 10% interval."

T33. Line 268-270: " Towards the end of the simulation, SW radiation interrupts the LW cooling effect increasingly as the solar angle increases, the SW radiation flux increases, however, not enough to result in neutral heating". Is punctuation missing? I find this sentence a little bit difficult to understand.

Response:
The sentence was revised to following to have better flow:

Location in revised manuscript: Sect. 3.1, p. 14, lines 305–314.

"SW warming reduces the net cloud top cooling increasingly as the solar angle increases, however, not enough to result in net warming."

T34. Line 273: "...over wider layer and..." – " . . . over a wider layer and . . . "

Response:
Modified as suggested.

Location in revised manuscript: Sect. 3.1, p. 14, lines 305–314.

T35. Line 274: ". . . in the Fig. 7." – ". . . in Fig. 7."

Response:
Modified as suggested.

Location in revised manuscript: Sect. 3.1, p. 14, lines 305–314.

T36. Line 279: "At 10.5 km level, in the middle vertically of the CONV layer. . . " – "At 10.5 km level, in the middle of the CONV layer" ?

Response:
Modified as suggested.

Location in revised manuscript: Sect. 3.1, p. 15, lines 315–320.

T37. Line 290: " in the Fig. 8" – " in Fig. 8"

Response:
Modified as suggested.

Location in revised manuscript: Fig. 8 discussion and caption, p. 15, lines 320–325.

T38. Line 302: "We compare here the. . . " – "We compare the. . . "

Response:
Modified as suggested.

Location in revised manuscript: Sect. 3.2, p. 16, lines 335–340.

T39. Line 303: "measured dusty cirrus layer" – "measured the dusty cirrus layer"

Response:
Modified as suggested.

Location in revised manuscript: Sect. 3.2, p. 16, lines 335–340.

T40. Line 316: "SEDI layer. . . " – "the SEDI layer".

Response:
Modified as suggested.

Location in revised manuscript: Sect. 3.2, pp. 17–18, lines 355–380.

T41. Line 316: "ice production in temperature range. . . " – "ice production in the temperature range. . . "

Response:
Modified as suggested.

Location in revised manuscript: Sect. 3.2, pp. 17–18, lines 355–390.

T42. Line 320: "... roughly same for total ICNC." – "... roughly the same for total ICNC".

Response:
Modified as suggested.

Location in revised manuscript: Sect. 3.2, pp. 17–18, lines 370–380.

T43. Figure 10:

T43a. in panel b, there is a red dashed line that according to the legend correspond to the OCP measurements. Shouldn't it be a solid red line corresponding to NIXE-CAPS instead?

Response:
Thank you for pointing out. Lines are now fixed accordingly. Please refer to Fig. 1 under response to RC1-G1.

Location in revised manuscript: Fig. 9 caption, p. 17, lines 365–370.

T43b. Since it is mentioned in the discussion, it could be helpful to add also in the panels (or at least in one panel) the lines corresponding to CONV and SEDI.

Response:
CONV and SEDI lines added.

Location in revised manuscript: Fig. 9 caption, p. 17, lines 365–370.

T43c. Please review this caption as it mentions "Model ICNC" when it should be IWC and the description of some of the lines does not match the legend.

Response:
Thank you for pointing out. Fixed.

Location in revised manuscript: Fig. 9 caption, p. 17, lines 365–370.

T44. Line 326: if the authors agree, instead of adding the abbreviation ISD in the text, "ice PSD" could be kept and in the caption of Fig. 11 add the meaning of ISD as it is done with INS and SOL.

Response:
We have modified accordingly so that we do not use terminology ISD within the text. We now use ice PSD instead. We have kept the use of ISD inside new Fig. 10.

Location in revised manuscript: Fig. 10 caption, p. 19, lines 400–405.

T45. Line 332: "The large number of ice below 30 μm" – "The large number of ice below 30 μm in Fig. 11a"

Response:
Modified as suggested.

Location in revised manuscript: Sect. 3.2, p. 18, lines 385–395.

T46. Line 336: "For the Fig. 11," – "For Fig. 11,"

Response:
Modified as suggested.

Location in revised manuscript: Sect. 3.2, p. 18, lines 385–395.

T47. Figure 11:

T47a. for clarity, or in the title of each panel or in the caption, it would be helpful to add which panel correspond to which ND.

Response:
Added ND titles to new Figs. 10 and 13. Please find the figures as Fig. 7 under RC1-S19 and as Fig. 3 under RC1-G2.

Location in revised manuscript: Fig. 10 caption, p. 19, and Fig. 13 caption, p. 22, lines 400–405 and 465–470.

T47b. Please, review the legend in panel a. Some of the lines have the wrong description.

Response:
Thank you for suggestions. The colors, markers and linestyles were all additionally modified to improve readability.

Location in revised manuscript: Fig. 10 caption, p. 19, lines 400–405.

T48. Line 348-350: " with ICNC only exceeding 10^{-2} cm^{-3} but with substantially weaker nucleation activity." I think the use of "but" can confuse the reader.

Response:
Modified as suggested. We replaced but with "and"

Location in revised manuscript: Sect. 3.3.1, p. 19, lines 405–415.

T49. Figure 13:

T49a. I think it is a bit difficult to differentiate the ICNC contours. If it looks better, I would suggest a change to a lighter color.

T49b. Please, specify or in the panel titles or in the caption which ND corresponds to which panel.

Response:
We have changed the contour lines to a lighter grey and reduced their width. We have also added N_D titles to each panel.

Location in revised manuscript: Fig. 13 caption, p. 22, lines 465–470.

T50. Line 389: the author refer to Fig. 13 (color code RHi) when the text is explaining LW cooling. Is this correct?

Response:
We have added arrows to Fig. 13 at hourly intervals indicating LW, SW, and net radiative heating/cooling rates. Please find the Fig. 3 under RC1-G2.

Location in revised manuscript: Fig. 13 caption, p. 22, lines 465–470.

T51. Line 400: "ICNC increases..." –"ICNC (Fig. 14a) increases..."

Response:
Thank you.

Location in revised manuscript: Sect. 3.4, p. 25, lines 520–525.

T52. Line 402: "The IWC on..." – "The IWC (Fig. 14e) on..."

Response:
Modified as suggested.

Location in revised manuscript: Sect. 3.4, p. 25, lines 520–525.

T53. Line 405: "gradient dθ_e/dz..." – "gradient dθ_e/dz... (Fig. 14b)"

Response:
Modified as suggested.

Location in revised manuscript: Sect. 3.4, p. 25, lines 520–525.

T54. Line 408: "the Fig. 9" – "Fig. 9"

Response:
Modified as suggested.

Location in revised manuscript: Sect. 3.4, p. 25, lines 520–530.

T55. Line 409: " The smaller the value of $\partial\theta_e/\partial z$ that seems to be below 0" seems?

Response:
The sentence was restructured part of large overhaul of Section 3.4 (was 3.2.1). Now it reads:

Location in revised manuscript: Sect. 3.4, p. 25, lines 520–530.

"For $N_D \geq 1$ cm^{-3}, negative values of $\partial\theta_e/\partial z$ are found within the CONV layer, indicating that radiative cooling (Fig. 15d) is sufficient to generate conditional instability. For $N_D < 1$ cm^{-3}, $\partial\theta_e/\partial z$ becomes positive, supporting the interpretation presented in Fig. 13 that the generation of new convective cells is no longer sustained."

T56. Line 410: "Fig. 14" – "Fig. 14F"

Response:
Modified as suggested.

Location in revised manuscript: Fig. 15 caption and Sect. 3.4, p. 25, lines 520–530.

T57. Line 420: "When expressed in terms of mass concentration rather than number concentration ND (Fig.14)" – "When expressed in terms of mass concentration rather than number concentration ND as was shown in Fig. 14,"

Response:
Modified as suggested.

Location in revised manuscript: Sect. 3.4, p. 26, lines 540–550.

T58. Figure 14:

T58a. Y label of panel d): radiative cooling/heating rate

T58b. In the caption: "c) Radiative..." .. "c) radiative ..."

T58c. Do the up triangles and down triangles in panel c) mean anything in particular?

T58d. "RHi is shown with with..." one "with" too much.

T58e. For consistency, I would suggest using also circles in panel e).

T58f. In line 399 is mentioned that Fig. 14 shows the relationships between the ND and bulk cirrus properties at the end of the simulations. In the caption it is written " The ND corresponds to initial concentration at the beginning of simulations between 8.5 and 11 km altitude". Could the authors clarify what is shown in the x-axis?

Response:
We thank the referee for the detailed comments on Figure 14. The figure has been substantially redesigned and is shown part of response to referee 1 and is labeled as Figure 3 and shown here as Fig. 8 under RC1-S24. We have taken into account the feedback on specific points in the revised figure. We have not used the SW warming and LW cooling lines in the revised figure, and instead show vertical profiles. In this form, it is easier to understand how the net radiative balance vertically affects the dusty cirrus formation in each case. Also, instead of using N_D as the x-axis in the panels, we have changed the N_D and C_D to the legend.

Location in revised manuscript: Figs. 14–16 and Sect. 3.4, pp. 24–26, lines 505–550.

T59. Line 431: "(Fig 14)" – "(Fig 14d)". If the authors consider it convenient, it could be also mentioned that in the supplement are figures for the LW, SW and net radiative rates.

Response:
We added mentions of Supplementary figures.

Location in revised manuscript: Fig. 16 caption, p. 26, lines 545–550.

T60. Line 432-433: "RHi also exhibits a dependence on ND , where the RHi variability within the CONV decreases as ND is increased, meaning that RHi is suppressed by frequent DIN events". I would suggest moving this line to the discussion about RHi initiated in line 416.

Response:
This part was removed since RHi is already discussed extensively earlier.

T61. Figure 15: missing in the caption the explanation of the black line.

Response:
Modified as suggested. Please find the added text in the following:

Location in revised manuscript: Fig. 15 caption, p. 25, lines 520–525.

"Black line corresponds to the total fit to the OPC data previously shown in Fig. 16"

T62. Line 440: "Two simulations representing nighttime and daytime simulations... " – "Two simulations representing nighttime and daytime... "

Response:
Modified as suggested.

Location in revised manuscript: Sect. 3.5, p. 27, lines 550–565.

T63. Figure 16: since it is mentioned in the discussion of this figure, I would suggest to add again in one of the plots the lines for CONV and SEDI.

Response:
Added CONV, SEDI and TP text on the altitude axis. The CONV, SEDI and TP threshold levels are quite dynamic and vary over time and thus they have been marked on the side of shared y-axis between panels at approximate levels where each levels are located at. Please see the Fig. 10 under RC1-S32.

Location in revised manuscript: Fig. 17 caption, p. 28, lines 580–585.

T64. Line 471-472: " DARDAR-Nice observations at 12 UTC show maintained high ICNC and IWC (corresponding to hour 10 in LES time (Fig. 10))" I would suggest rewriting this sentence, perhaps: "As shown in Fig. 10, DARDAR-Nice observations at 12 UTC show maintained high ICNC and IWC (corresponding to hour 10 in LES time (Fig. 16))"

Response:
Modified as suggested.

Location in revised manuscript: Sect. 3.5.1, p. 28, lines 585–595.

T65. Figure 17: if it looks clearer, I would suggest also here change the color of the contour lines.

Response:
Modified new Fig. 19 so that contour lines are thinner and grey. This make it easier to see where the contour lines are located over the dark background shading. Figure 17 shown below.

Location in revised manuscript: Fig. 19 caption, p. 30, lines 615–620.

T66. Figure 19: it could help the reader to see the CONV lines also in one of these plots.

Response:
CONV, SEDI and TP lines added to the current Fig. 20. Please see Fig. 11 under RC1-S34.

Location in revised manuscript: Fig. 20 caption, p. 31, lines 635–640.

T67. Data availability: shouldn't be also mentioned in this section where to find the DARDAR data?

Response:
Added source for DARDAR data as following:

Location in revised manuscript: Code and data availability, pp. 32–33, lines 680–690.

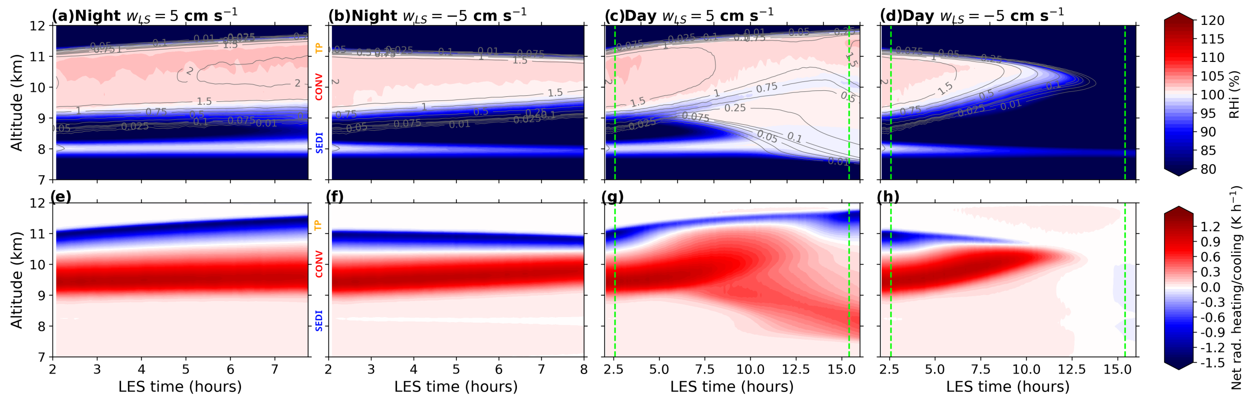

Figure 17: RHi in shading and ICNC (cm^{-3}) in contours (a-d) and net radiative heating rate in shading (e-h). Panels (a,e) and (b,f) represent nighttime simulations with (a,e) $w_{LS} = 5$ cm s^{-1} and (b,f) $w_{LS} = -5$ cm s^{-1}. The same applies respectively for (c,g) and (d,h) in daytime simulations.

"DARDAR-Nice data is available from data repository of University of Lille at https://www.icare.univ-lille.fr/dardar/"

T68. Add CONV/SEDI lines to Figures 16 and 19

Response:
Modified accordingly. See the responses RC2-T63 and RC2-T66

Location in revised manuscript: Figs. 17 and 19 captions, pp. 28 and 30, lines 580–585 and 615–620.

T69. Line 563: instead of "https://github.com/UCLALES-SALSA/ UCLALES-SALSA under release tag dustycirrus." I would suggest to write https://github.com/UCLALES-SALSA (without / at the end) so the link works (without /) or directly: https://github.com/UCLALES-SALSA/UCLALES- SALSA/tree/dustycirrus

Response:
Modified as suggested. Modified accordingly.

Location in revised manuscript: Code and data availability, p. 33, lines 685–690.

T70. Line 598: instead of introducing the term AIDA in line 626, I would recommend to introduce it here.

Response:
Introduction of AIDA was moved under Hiranuma et al. 2014 text:

Location in revised manuscript: Appendix C, p. 38, lines 735–740.

"The heterogeneous ice nucleation parameterization of Hiranuma et al. (2014) is based on laboratory measurements conducted in the Aerosol Interaction and Dynamics in the Atmosphere (AIDA) cloud chamber,..."

T71. Figure B1:

T71a. Title of the middle panel should be "Ulricht et al. (2017)"

Response:
Modified as suggested. Please see Fig. 12 under response to RC1-T2.

Location in revised manuscript: Fig. C1 caption, p. 38, lines 730–735.

T71b. I personally find the size of the labels a bit smaller. I would recommend making them larger.

Response:
Size of the labels have been increased for readability.

Location in revised manuscript: Fig. C1, p. 38, lines 730–735.

T72. Line 645: nINP, X instead of nX ?

Response:
Corrected as:

Location in revised manuscript: Appendix C, p. 40, lines 770–775.

"where $n_{\mathrm{INP},X}$ is the INP number concentration and μ_X is the mean number of ice embryos..."

T73. Figure B2: same comment as for Fig. B1 regarding the size of the labels.

Response:
Size of the labels have been increased.

Location in revised manuscript: Fig. C2 caption, p. 41, lines 800–805.

REFERENCES

Calderón, S. M., Hyttinen, N., Kokkola, H., Raatikainen, T., Lawson, R. P., and Romakkaniemi, S.: Secondary ice formation in cumulus congestus clouds: insights from observations and aerosol-aware large-eddy simulations, Atmospheric Chemistry and Physics, 25, 14 479–14 500, https://doi.org/10.5194/acp-25-14479-2025, 2025.

Froyd, K., Yu, P., Schill, G., Brock, C., Kupc, A., Williamson, C., Jensen, E., Ray, E., Rosenlof, K., Bian, H., Darmenov, A., Colarco, P., Diskin, G., Bui, T., and Murphy, D.: Dominant role of mineral dust in cirrus cloud formation revealed by global-scale measurements, Nature Geoscience, 15, 1–7, https://doi.org/10.1038/s41561-022-00901-w, 2022.

Fu, Q. and Liou, K. N.: Parameterization of the Radiative Properties of Cirrus Clouds, Journal of Atmospheric Sciences, 50, 2008 – 2025, https://doi.org/10.1175/1520-0469(1993)050⟨2008:POTRPO⟩2.0.CO;2, 1993.

Hersbach, H., Bell, B., Berrisford, P., Hirahara, S., Horányi, A., Muñoz-Sabater, J., Nicolas, J., Peubey, C., Radu, R., Schepers, D., Simmons, A., Soci, C., Abdalla, S., Abellan, X., Balsamo, G., Bechtold, P., Biavati, G., Bidlot, J., Bonavita, M., De Chiara, G., Dahlgren, P., Dee, D., Diamantakis, M., Dragani, R., Flemming, J., Forbes, R., Fuentes, M., Geer, A., Haimberger, L., Healy, S., Hogan, R. J., Hólm, E., Janisková, M., Keeley, S., Laloyaux, P., Lopez, P., Lupu, C., Radnoti, G., de Rosnay, P., Rozum, I., Vamborg, F., Villaume, S., and Thépaut, J.-N.: The

ERA5 global reanalysis, Quarterly Journal of the Royal Meteorological Society, 146, 1999–2049, https://doi.org/https://doi.org/10.1002/qj.3803, 2020.

Hiranuma, N., Paukert, M., Steinke, I., Zhang, K., Kulkarni, G., Hoose, C., Schnaiter, M., Saathoff, H., and Möhler, O.: A comprehensive parameterization of heterogeneous ice nucleation of dust surrogate: laboratory study with hematite particles and its application to atmospheric models, Atmospheric Chemistry and Physics, 14, 13 145–13 158, https://doi.org/10.5194/acp-14-13145-2014, 2014.

Jacobson, M. Z.: Fundamentals of Atmospheric Modeling, Cambridge University Press, 2 edn., 2005.

Kollath, K.: Cellular convection in cirrus clouds as a possible effect of dust aerosols, `https://www.eumetsat.int/media/46886`, eUMETSAT, last access: 30 October 2022, 2010.

Koop, T., Luo, B., Tsias, A., and Peter, T.: Water Activity as the determinant for homogeneous ice nucleation in aqueous solutions, Nature, 406, 611–4, https://doi.org/10.1038/35020537, 2000.

Krämer, M., Rolf, C., Spelten, N., Afchine, A., Fahey, D., Jensen, E., Khaykin, S., Kuhn, T., Lawson, P., Lykov, A., Pan, L. L., Riese, M., Rollins, A., Stroh, F., Thornberry, T., Wolf, V., Woods, S., Spichtinger, P., Quaas, J., and Sourdeval, O.: A microphysics guide to cirrus – Part 2: Climatologies of clouds and humidity from observations, Atmospheric Chemistry and Physics, 20, 12 569–12 608, https://doi.org/10.5194/acp-20-12569-2020, 2020.

Kärcher, B., Hoffmann, F., Sokol, A., Gasparini, B., Corcos, M., Jensen, E., Atlas, R., Podglajen, A., Morrison, H., Hertzog, A., Plougonven, R., Chandrakar, K., and Grabowski, W. W.: Dissecting cirrus clouds: navigating effects of turbulence on homogeneous ice formation, npj Climate and Atmospheric Science, 8, https://doi.org/10.1038/s41612-025-01024-w, 2025.

Lawson, R. P., Woods, S., Jensen, E., Erfani, E., Gurganus, C., Gallagher, M., Connolly, P., Whiteway, J., Baran, A. J., May, P., Heymsfield, A., Schmitt, C. G., McFarquhar, G., Um, J., Protat, A., Bailey, M., Lance, S., Muehlbauer, A., Stith, J., Korolev, A., Toon, O. B., and Krämer, M.: A Review of Ice Particle Shapes in Cirrus formed In Situ and in Anvils, Journal of Geophysical Research: Atmospheres, 124, 10 049–10 090, https://doi.org/https://doi.org/10.1029/2018JD030122, 2019.

Nagy, A.: Investigating weather situations which bring Saharan dust over Hungary based on MSG satellite images, Master's thesis, ELTE University, 2009.

NASA: MODIS/Terra Atmospherically Corrected Surface Reflectance Product (MOD09) [data set], https://doi.org/10.5067/MODIS/MOD09.061, level-2 atmospheric-corrected surface reflectance (MOD09 series), 2015.

Phillips, V. T. J., Demott, P. J., Andronache, C., Pratt, K. A., Prather, K. A., Subramanian, R., and Twohy, C.: Improvements to an Empirical Parameterization of Heterogeneous Ice Nucleation and Its Comparison with Observations, Journal of the Atmospheric Sciences, 70, 378 – 409, https://doi.org/10.1175/JAS-D-12-080.1, 2013.

Pieper, L., Seifert, P., Griesche, H., Ansmann, A., McCosh, G., Ewald, F., and Kneifel, S.: Turbulence structure of dusty cirrus and its relation to atmospheric conditions: A characterization using cloud-radar measurements and reanalysis data, EGUsphere, 2026, 1–38, https://doi.org/10.5194/egusphere-2026-3092, 2026.

Protat, A. and Williams, C. R.: The Accuracy of Radar Estimates of Ice Terminal Fall Speed from Vertically Pointing Doppler Radar Measurements, Journal of Applied Meteorology and Climatology, 50, 2120 – 2138, https://doi.org/10.1175/JAMC-D-10-05031.1, 2011.

Ren, C. and Mackenzie, A. R.: Cirrus parametrization and the role of ice nuclei, Quarterly Journal of the Royal Meteorological Society, 131, 1585–1605, https://doi.org/https://doi.org/10.1256/qj.04.126, 2005.

Seifert, A., Bachmann, V., Filipitsch, F., Förstner, J., Grams, C. M., Hoshyaripour, G. A., Quinting, J., Rohde, A., Vogel, H., Wagner, A., and Vogel, B.: Aerosol–cloud–radiation interaction during Saharan dust episodes: the dusty cirrus puzzle, Atmospheric Chemistry and Physics, 23, 6409–6430, https://doi.org/10.5194/acp-23-6409-2023, 2023.

Smagorinsky, J.: GENERAL CIRCULATION EXPERIMENTS WITH THE PRIMITIVE EQUATIONS: I. THE BASIC EXPERIMENT, Monthly Weather Review, 91, 99 – 164, https://doi.org/10.1175/1520-0493(1963)091⟨0099:GCEWTP⟩2.3.CO;2, 1963.

Sourdeval, O., Gryspeerdt, E., Krämer, M., Goren, T., Delanoë, J., Afchine, A., Hemmer, F., and Quaas, J.: Ice crystal number concentration estimates from lidar–radar satellite remote sensing – Part 1: Method and evaluation, Atmospheric Chemistry and Physics, 18, 14 327–14 350, https://doi.org/10.5194/acp-18-14327-2018, 2018.

Sölch, I. and Kärcher, B.: A large-eddy model for cirrus clouds with explicit aerosol and ice microphysics and Lagrangian ice particle tracking, Quarterly Journal of the Royal Meteorological Society, 136, 2074–2093, https://doi.org/https://doi.org/10.1002/qj.689, 2010.

Ullrich, R., Hoose, C., Möhler, O., Niemand, M., Wagner, R., Höhler, K., Hiranuma, N., Saathoff, H., and Leisner, T.: A New Ice Nucleation Active Site Parameterization for Desert Dust and Soot, Journal of the Atmospheric Sciences, 74, 699 – 717, https://doi.org/10.1175/JAS-D-16-0074.1, 2017.

Weger, M., Heinold, B., Engler, C., Schumann, U., Seifert, A., Fößig, R., Voigt, C., Baars, H., Blahak, U., Borrmann, S., Hoose, C., Kaufmann, S., Krämer, M., Seifert, P., Senf, F., Schneider, J., and Tegen, I.: The impact of mineral dust on cloud formation during the Saharan dust event in April 2014 over Europe, Atmospheric Chemistry and Physics, 18, 17 545–17 572, https://doi.org/10.5194/acp-18-17545-2018, 2018.

Westbrook, C. D., Hogan, R. J., and Illingworth, A. J.: The Capacitance of Pristine Ice Crystals and Aggregate Snowflakes, Journal of the Atmospheric Sciences, 65, 206 – 219, https://doi.org/10.1175/2007JAS2315.1, 2008.

Table 1: List of abbreviations used in this study.

Abbreviation	Description
ACTRIS	Aerosol, Clouds and Trace Gases Research Infrastructure
AERORAD	Aerosol radiation scheme
BAHAMAS	The Basic HALO Measurement and Sensor System
BASE	Reference simulation
BASE-MIXED	Reference simulation including mixed aerosol conditions
CET	Cloud effective temperature
CONV	Convective layer of the dusty cirrus
DARDAR-Nice	Radar–lidar cloud retrieval ice product
DIN	Deposition ice nucleation
ERA5	ECMWF Reanalysis version 5
HALO	High Altitude and Long Range Research Aircraft
H14	Hiranuma et al. (2014) DIN parameterization
ICNC	Ice crystal number concentration
INAS	Ice nucleation active site density
INP	Ice nucleating particle
INS	Ice nucleating particle distribution
IWC	Ice water content
LES	Large-Eddy Simulation
LW	Longwave radiation
ML-CIRRUS	Mid-Latitude Cirrus campaign
MODIS	Moderate Resolution Imaging Spectroradiometer
MSG	Meteosat Second Generation
NIXE-CAPS	NIXE Cloud and Aerosol Particle Spectrometer
OPC	Optical Particle Counter
P13	Phillips et al. (2013) DIN parameterization
PSD	Particle size distribution
RHi	Relative humidity with respect to ice
SALSA	Sectional Aerosol module for Large Scale Applications
SEDI	Sedimentation-dominated layer
SEVIRI	Spinning Enhanced Visible and Infrared Imager
SOL	Soluble aerosol distribution
SW	Shortwave radiation
U17	Ullrich et al. (2017) DIN parameterization
UCLALES	University of California Los Angeles Large-Eddy Simulator
UTC	Coordinated Universal Time

Table 2: Symbols and variables used in this study.

Symbol	Description	Unit
c_d	Dust mass concentration	μg m^{-3}
D_i	Ice particle diameter	μm
D_p	Aerosol particle diameter	μm
IWC	Ice water content	g m^{-3}
$ICNC$	Ice crystal number concentration	cm^{-3}
N_D	Dust number concentration	cm^{-3}
RHi	Relative humidity with respect to ice	%
T	Temperature	K
w	Vertical velocity	m s^{-1}
w_{LS}	Large-scale vertical velocity	cm s^{-1}
z	Altitude	km
θ_e	Equivalent potential temperature	K
$\partial\theta_e/\partial z$	Vertical gradient of equivalent potential temperature	Kkm^{-1}
σ_{RHi}	Standard deviation of RHi	%

Dataset	Layer	IWC (mg m^{-3})	ICNC (cm^{-3})
		Mean $\pm$ SD	Mean $\pm$ SD
NIXE-CAPS	CONV	22.45 $\pm$ 5.47	2.39 $\pm$ 0.33
	SEDI	26.82 $\pm$ 8.75	1.87 $\pm$ 0.40
DARDAR-Nice	CONV	19.22 $\pm$ 10.85	0.62 $\pm$ 0.42
	SEDI	16.77 $\pm$ 8.40	0.23 $\pm$ 0.15
MIRA-35C	CONV	9.03 $\pm$ 5.93	—
	SEDI	5.20 $\pm$ 2.71	—
BASE	CONV	29.15 $\pm$ 5.44	1.23 $\pm$ 0.22
	SEDI	28.63 $\pm$ 4.98	0.24 $\pm$ 0.04
BASE-MIXED	CONV	29.34 $\pm$ 3.76	1.92 $\pm$ 0.31
	SEDI	24.75 $\pm$ 3.95	0.25 $\pm$ 0.04

Table 3: IWC and ICNC statistics for the convective (CONV) and sedimentation (SEDI) layers. Values are mean $\pm$ standard deviation. NIXE-CAPS measurements cover up to 9.5 km which does not cover the whole CONV layer. DARDAR-Nice covers data at 12:30 UTC between 47° and 49°N latitude over a trajectory shown in Fig. 14. MIRA-35C covers IWC estimates between 06:00 and 08:00 UTC at Schneefernerhaus, Germany.